Comparative single cell analysis reveals complex patterns of cell type and cell signaling innovations at the fetal-maternal interface

Daniel J. Stadtmauer*[1,2], Silvia Basanta*[3], Jamie D. Maziarz[1], Alison G. Cole[4], Gülay Dagdas[3], Gilbecca Rae Smith[5], Frank van Breukelen[5], Mihaela Pavličev[3,6], Günter P. Wagner [1,3,7]

* These authors contributed equally

1. Department of Ecology & Evolutionary Biology, Yale University, New Haven, CT, USA
2. Konrad Lorenz Institute for Evolution and Cognition, Klosterneuburg, Austria
3. Department of Evolutionary Biology, University of Vienna, Vienna, Austria
4. Department of Neuroscience and Developmental Biology, University of Vienna, Vienna, Austria
5. School of Life Sciences, University of Nevada, Las Vegas, Las Vegas, NV, USA
6. Complexity Science Hub Vienna, Vienna, Austria
7. Department of Animal Science, Texas A&M University, College Station, TX, USA

To whom correspondence may be addressed:

Daniel J. Stadtmauer daniel.stadtmauer@yale.edu

Silvia Basanta silvia.basanta@univie.ac.at

Mihaela Pavličev mihaela.pavlicev@univie.ac.at

Günter P. Wagner gunter.wagner@yale.edu

Abstract

The decidual-placental interface is one of the most diverse and rapidly evolving tissues in mammals. Its origin as a chimeric fetal-maternal tissue poses a unique evolutionary puzzle. We present single-cell RNA sequencing atlases from the fetal-maternal interfaces of the opossum, a marsupial, the Malagasy common tenrec, an afrotherian with primitive reproductive features, and mouse, guinea pig, and human. Invasive trophoblast shares a common transcriptomic signature across eutherians, which we argue represents a cell type family that radiated following the evolution of hemochorial placentation. We find evidence that the eutherian decidual stromal cell evolved stepwise from a predecidual state retained in *Tenrec*, followed by a second decidual cell type originating in Boreoeutheria with endocrine characteristics. We reconstruct ligand-receptor signaling to test evolutionary hypotheses at scale. Novel trophoblast and decidual cell types display strong integration into signaling networks compared to other cells. Additionally, we find consistent disambiguation between fetal and maternal signaling. Using phylogenetic analysis, we infer the cell-cell signaling network of the Placental common ancestor, and identify increased rates of signaling evolution in Euarchontoglires. Together, our findings reveal novel cell type identities and cell signaling dynamics at the mammalian fetal-maternal interface.

Introduction

The origin of novel cell types, tissues, and organs is essential for the evolution of complex multicellular organisms. However, our understanding of how evolution at these higher levels of organization relates to innovation at the cellular level is currently limited. One of the most intense loci of cell signaling in the body is the fetal-maternal interface, where cells from the fetal placenta invade into and establish intimate communication with the maternal endometrium. Placental invasion and the corresponding transformation of maternal tissues called decidualization first evolved in the stem lineage of placental mammals[1,2]. In this paper, we use this key evolutionary event to ask a fundamental question: how does a complex novelty such as the placental-decidual interface, composed of highly interdependent and novel constituent parts, come to be assembled by evolution?

Answering this question demands a comparative perspective. Single-cell transcriptomic atlases of the human placenta have yielded insight into the cell-cell interaction networks governing this unique chimeric organ[3–5]. However, the fetal-maternal interface is also one of the most rapidly evolving, and hence most diverse, characters among mammals. Here, we present and compare single-cell data from the fetal-maternal interface of five species at key points in mammal phylogeny. These are the gray short-tailed opossum, *Monodelphis domestica*, a non-deciduate marsupial with restricted placental invasion, and four eutherian species with divergent forms of invasive placenta: the Malagasy common tenrec *Tenrec ecaudatus*, an afrotherian mammal considered the most "primitive" form of hemochorial (invasive) placenta[6,7], and three Euarchontoglires with different patterns and degrees of placental invasiveness - the guinea pig *Cavia porcellus*, the mouse *Mus musculus*, and recently published data from *Homo sapiens*[4,5]. Afrotherian and marsupial outgroups allow us to bracket the phylogenetic spread of therian mammals beyond the well-studied Boreoeutheria (primates, rodents and hooved animals).

We establish putative cell type homologies across therian mammals, identifying invasive trophoblast subpopulations of guinea pig and tenrec which share a gene expression signature with human extravillous trophoblast, and discover a primitive predecidual cell type in the tenrec which suggests a stepwise evolution of the decidual stromal cell type. We reconstruct ancestral cell-cell signaling networks, revealing the integration of novel cell types into the interface. Finally, we test two long-standing theoretical predictions, the disambiguation hypothesis[8] and escalation hypothesis[9], for the first time at transcriptome-wide scale. In so doing, we trace the co-evolutionary history of cell types and cell signaling across the origin and subsequent diversification of mammalian placentation at single-cell resolution.

Results

Therian mammals differ in placental and uterine cell type inventories

Single-cell transcriptomic data were collected from the fetal-maternal interface (placenta, endometrium, and myometrium) of mammals at informative phylogenetic positions for the evolution of placentation. Samples were collected at homologous developmental stages following establishment of a definite placenta, after implantation and trophoblast differentiation and invasion had completed but before the physiological changes leading to the onset of parturition. Time points chosen were opossum day 13.5 of 14.5, mouse day 15.5 of 19-21, guinea pig day 30.5 of 62, and tenrec day 28-29 of 56. Data sets were analyzed following a standardized approach (**Suppl. Figure 1**). The resulting multi-species cell type atlases (**Figure 1a**) consist of 393,074 cells (67,409 cells excluding publicly available data), with an average of 9878 transcripts per cell. Cell clusters were identified using Leiden clustering and marker gene-based annotation. To reduce over- or under-clustering, we used non-negative matrix factorization (NMF)[10] to identify coregulated gene modules (**Suppl. Figure 2**). Cell clusters without uniquely distinguishable NMF gene modules or markers were merged. Finally, we used cell morphology and histological localization to refine cell type annotations. Detailed histological descriptions are provided in Supplementary Material.

Tissue organization (**Figure 1b**) and cell type composition (**Figure 1c**) differed across species. In the opossum, fetal-maternal cell contact and nutrient exchange occur in the same location, whereas in the four eutherian mammals studied, both a "vascular interface" where maternal circulation is made available to the fetus, and a "decidual-placental interface", where invading trophoblast makes maternal cell contact, are present. The latter was the focus of more detailed analysis due to greater potential for co-evolved cell-cell signaling. The opossum's fetal-maternal interface is a lamellar matrix of trophoblast which coats maternal luminal epithelium and uptakes glandular secretions (**Suppl. Figure 3a**). Uterine glands, which provide histotrophic nutrition, are expansive (**Figure 1b**); indeed, more than 50% of the cells captured in the opossum were epithelial, of which most (85%) were glandular (**Figure 1c**). Stromal cells such as fibroblasts were more scarce (8%) in opossum than in other species, allowing maternal vascular endothelium to lie in close proximity to trophoblast (**Figure 1b**). In the tenrec, mouse, and guinea pig, the vascular interface is a trophoblast labyrinth surrounding maternal blood (**Figure 1b; Suppl. Figure 3b**), whereas the human vascular interface consists of fetal villi reaching into a maternal blood sinus. In the tenrec, we identified large-diameter glands containing mucus and leukocytes, suggesting continued histotrophic nutrition (**Suppl. Figure 3b**), whereas in the other eutherians histotrophy had ceased by the time placental invasion was complete. Lymphoid cells, primarily NK-like innate cells, constituted 58% of the total cells recovered in this species (**Figure 1c**). The guinea pig, mouse, and human had similar cell type compositions (**Figure 1c**), with one notable structural difference: the guinea pig's decidual-placental interface took the form of a folded cytotrophoblast structure called the subplacenta, which anchors the placenta to the maternal decidua (**Figure 1b**) and gives rise to invasive trophoblast[11].

Assessment of cross-species homology between cell populations was assisted by self-assembling manifold mapping (SAMap)[12] (**Suppl. Tables 1-3; Suppl. Figure 4**). SAMap mapping scores clustered into reciprocally linked groups (**Figure 1d**). Conserved maternal cell types including smooth muscle, pericytes, leukocytes, endothelial, epithelial, and mesothelial cells showed consistent reciprocal similarity across species, making homology inference uncomplicated (**Figure 1d**). In contrast, trophoblast and decidual cell types displayed lower transcriptomic conservation across species, suggesting rapid gene expression evolution.

To obtain a global picture of cell type relationships including within-species hierarchical structure, we calculated a neighbor-joining phylogenetic tree of cell type transcriptomes. This yielded monophyletic or near-monophyletic groupings corresponding to major cell type families (**Figure 1e**; see **Methods**). The tree contained a hematopoietic cell clade with myeloid and lymphoid sub-groups, a clade of non-immune mesenchymal cells including endothelial cells, and a mixed epithelial/trophoblast clade. These cell type family groupings were largely maintained when the genes used to generate the phylogeny were restricted to transcription factors (**Suppl. Figure 5**), suggesting that the pattern reflects cell type regulatory identity and not solely phenotypic convergence[13]. The robustness of these cell type families justified the use of these categories to aggregate cells for phylogenetic analysis of gene expression (see **Figure 4**). Of these cell type families, those with the most cell type innovation in mammals, the trophoblast and endometrial stroma, were chosen for more detailed analysis.

Placental cell type homology and eutherian radiation of invasive trophoblasts

Trophoblast cell types are traditionally classified by topological location (e.g., extravillous), phenotype (e.g., glycogen trophoblast, syncytiotrophoblast), or ploidy (giant trophoblast), but whether these divisions correspond to cell type identities conserved across species has remained an unresolved question.

Human trophoblast cell types have been well documented by single-cell methods (**Figure 2a**)[5,14]: Cytotrophoblast of the placental villi (Hs_VCT) can undergo fusion, becoming syncytiotrophoblast (Hs_SCT; marked by steroidogenic enzymes *CYP11A1* and *CYP19A1*), or develop invasive properties becoming extravillous trophoblasts (EVT). EVTs can take an interstitial (Hs_iEVT) route into the decidua or an endovascular (Hs_eEVT) pathway to replace the maternal spiral artery

endothelium. EVT-lineage cells express genes including *ADAM19*, *MMP15*, *PLAC8*, *PTPRF*, *QSOX1*, and vascular growth factor receptor *FLT1* and *FLT4* (**Figure 2a**) which we used to assemble a "pan-invasive" gene set for comparison to other species. By analogy to human extravillous trophoblast, we refer to other species' trophoblast cells which migrate into the decidua as "extraplacental trophoblast" (EPT).

In the opossum, two trophoblast populations were identified (**Figure 2a**). Cytotrophoblast (Md_CTB) expressed transcription factors *WFDC2* and *ZBTB7C*, the keratin *KRT7*, desmosome components *DSC2* and *DSG2*, and the t-SNARE protein *SNAP25* involved in vesicle fusion[15]. Indeed, opossum trophoblast cells uptake apocrine secretory bodies from the maternal epithelium (**Suppl. Figure 3a**). We localized the transcription factor *HAND1* to mononuclear cells in the trophectoderm as well as to fetal mesenchymal cells (**Figure 1b**). The second trophoblast cell cluster expressed syncytiotrophoblast transcription factors *GCM1* and *DLX3*[16], the cathepsins *CTSV* and *CTSH*, serine proteases *PRSS22* and *PRSS36*, high levels of the growth factor *VEGFA* (1494 transcripts per million). These cells also expressed the inflammatory mediators *IL1A*, *IL6*, *IL17A* and *PTGES*. *GCM1* and *IL6* expression, as well as *IL17A* as we recently reported[17], was restricted to diploid giant cells of the trophectoderm termed syncytial knots[18] (**Figure 2b**): we therefore name this cell type *GCM1+* syncytium (Md_SCT-GCM1). The placental origin of these cytokines was verified by comparison to laser-microdissected samples (**Suppl. Figure 6**). Previously it was discovered, via bulk sequencing, that opossum placentation entails upregulation of pro-inflammatory cytokines, from which the most parsimonious interpretation was an inflammatory response by the maternal endometrium[19,20]. However, the single-cell evidence here reveals that the inflammatory cytokine production and angiogenic signaling (*VEGFA*) is instead produced by a placental cell type, which appears to act as the main signaling hub in the opossum trophoblast.

In the tenrec we identified four distinct trophoblast populations (**Figure 2a**). One trophoblast cluster (Te_CTB-CYP11A1) expressed *CYP11A1*, the enzyme responsible for the first step in steroid production[21], which we localized to the superficial-most trophoblast coating the endometrium (**Figure 2b**). These cells also expressed heme oxidase *HMOX1*, and indeed catabolism of hemoglobin from maternal erythrocytes has been reported in the tenrec[22]. Another steroidogenic trophoblast cluster expressed the progesterone synthase *HSD3B1* and the cortisol/cortisone converting enzyme *HSD11B1* (Te_CTB-HSD3B1). A non-steroidogenic trophoblast cell type (Te_CTB-IGF2) expressed *WFDC2*, *FREM2*, *GPX2*, *SLC12A2*, and the somatotropin *IGF2*, although no expression of *prolactin* or other growth hormone paralogs was found. Putatively invasive trophoblast (Te_EPT), exhibiting SAMap linkage to human Hs_eEVT and Hs_GC, expressed *ADAMTS18*, *JADE3*, *JAZF1*, *PAPPA2*, *QSOX1*, cholesterol transporter *GRAMD1B* and cell invasion regulators *SCAI*[23] and *ZEB1*[24]. Cells expressing the placental proteoglycan GPC1, transcribed by Te_EPT and Te_CTB-HSD3B1, were found surrounding the deepest maternal vasculature (**Figure 2b**), suggesting that the *Tenrec ecaudatus* placenta is more invasive than reported for other tenrec species[25].

In the guinea pig, seven putative trophoblast cell clusters were distinguished, all belonging to the subplacenta and its invasive migrants as the labyrinth was removed prior to sample preparation (**Figure 1b**). Trophoblast took both interstitial and endovascular pathways, as KRT7^{+} trophoblast cells were present in the decidua, as well as surrounding maternal vasculature (**Suppl. Figure 3d**). Cells identified as extraplacental trophoblast (Cp_iEPT) expressed *CXCL12*, *PENK*, *FLT1*, *IL34*, and *ADAM19*, as well as the genes *QSOX1*, *CNFN*, and *GPC1*, which were shared with human endovascular EVT and mouse spiral artery-remodeling giant cells (**Figure 2a**). *GPC1* has been identified in the most deeply invasive trophoblast of the rat[26] and linked to angiogenesis and invasion[27]: we observed GPC1^{+} cells, likely Cp_iEPT, close to the maternal vasculature and the myometrium (**Figure 2b**). Another extraplacental cell cluster was distinguished by specific expression of *oxytocin* (Cp_EPT-OXT). A related subpopulation of likely invasive cell progenitors (Cp_EPT-CCC) shared expression of proliferation regulators *DLX5*[28] and *HMGA1* with human Hs_VCT_CCC; indeed, stem cell aggregations in the guinea pig subplacenta have been identified as homologs to the human cell column[29]. RNA velocity-informed pseudotime analysis[30] supported Cp_EPT-CCC cells as the most likely initial cell state of other trophoblast subsets (**Suppl. Figure 7**). Non-invasive trophoblasts shared the expression of the genes *CTSE*, *CXCL14*, *GJB2*, and *TMEM213* (**Figure 2a**). One sub-population

was enriched for *GDF15* (CTB-GDF15). Lastly, syncytiotrophoblast (Cp_SCT) expressed three paralogs of human *prolactin* and two of *LCN2*, as well as the transcription factors *GATA2*, *GATA3*, *TFAP2A, and TFAP2C*. TFAP2C was expressed in invasive syncytiotrophoblast "tongues", which derive from subplacental cytotrophoblast and invade deeply into the decidua[11] (**Figure 2b; Suppl. Figure 3e**). A different *prolactin* ortholog has been previously localized to the trophospongium in this species[31]. We histologically identified two populations of syncytium: invasive SCT, which derives from subplacental cytotrophoblast and invades up to the myometrium, and coarse-meshed SCT between the subplacenta and the labyrinth. Finally, giant trophoblast cells were histologically identified between the subplacenta and labyrinth and invading the decidua (**Suppl. Figure 3f**). However, due to their large size, these were not captured in the single-cell transcriptomes.

Mouse trophoblast cell populations included spongiotrophoblast, syncytiotrophoblast, labyrinth cytotrophoblast cells, and five populations of giant cells (**Figure 2a**). We confirmed cell annotation based on published markers[32,33]. Placental labyrinth markers *Cited1*, *Ctsj*, *Peg10*, *Rhox6*, *Rhox9*, and *Sin3b* had broad expression in the cells belonging to the labyrinth (Mm_SCT, Mm_TGC-C, Mm_TGC-S). Syncytiotrophoblast-I (Mm_SCT) expressed *Slc16a1*, *Hsd11b2*, and the syncytin *Syna*, a marker of the syncytiotrophoblast layer closest to the maternal vasculature[34]. Spongiotrophoblast (Mm_SPT) expressed the prolactin paralogs *Prl3a3* and *Prl3c1*[35], and a large number of pregnancy-specific glycoproteins (*Psg17*, *Psg18*, *Psg19*, *Psg25*, and *Psg28*, *Ceacam5* and *Ceacam13)*. Giant cells (TGC) were divided into invasive (iTGC) and noninvasive populations. Three clusters of invasive TGC were united by the expression of *Cdx2*, *Pcdh12*, *Plac1*, and *Tfap2c*. A progenitor invasive trophoblast subpopulation (Mm_TGC-Prog) was enriched for *Ascl2*, *Ldoc1*, and *Prdm1*[36], interstitially invasive glycogen trophoblast (Mm_TGC_Gly) was enriched in *Arid3a*, and endovascularly invasive spiral artery-remodeling giant cells (Mm_TGC-SpA) expressed the prolactins *Prl2a1* and *Prl7b1*. Lastly, noninvasive sinusoidal giant cells (Mm_TGC_S) were marked by *Prl2c2*, *Prl3b1*, and *Prl7d1*[37], and canal giant cells (Mm_TGC_C) were marked by *Hand1* and *Prl2c1*.

Besides trophoblast, we recovered cells from the yolk sac, placental mesenchyme, and fetal vasculature. Yolk sac endoderm was distinguished by widely-conserved amniote yolk sac markers[38] including alpha-fetoprotein *AFP* and apolipoproteins *APOA1*, *APOA2*, and *APOA4* (**Figure 2a**). Amniotic cells in the opossum, mouse and tenrec expressed *GABRP* and *VTCN1*[39]. Opossum and tenrec both exhibited a fetal mesenchymal cell type enriched in *HAND1*, *TBX20*, and *LIFR*, which in opossum appeared to be located near the placental vasculature (**Figure 2b**). This cell type was not identified in the Euarchontoglires species. Two other fetal mesenchymal cell types were identified in the tenrec, one enriched in the growth factor *FGF19* and another marked by corticotropin-releasing hormone *CRH*.

Inferring the evolutionary history of trophoblast cell types

We inferred fine-grained relationships among trophoblasts by building a network of SAMap scores and identifying reciprocally linked cell clusters through Leiden community detection (**Figure 2c**). The Leiden algorithm grouped the 29 trophoblast cell populations into five communities which represent putative homology groups. Two of the resulting communities consisted of invasive cell types and three included the noninvasive cell types (**Figure 2d**).

The two trophoblast cell types in our marsupial outgroup, the opossum, fell into different homology groups. The community to which opossum syncytial knot cells (Md_SCT-GCM1) were assigned contained extraplacental trophoblasts from tenrec (Te_EPT), guinea pig (Cp_iEPT), and human (Hs_GC, Hs_eEVT). On the other hand, opossum cytotrophoblast (Md_CTB) fell into a community containing trophoblast from each of the eutherian species sampled - tenrec cytotrophoblast (Te_CTB-HSD3B1), mouse sinusoidal trophoblast (Mm_TGC_S), guinea pig subplacental progenitors (Cp_EPT-CCC), and human villous cell column progenitors (Hs_VCT-CCC). This could indicate that the earlier developmental stages of eutherian cytotrophoblast and marsupial cytotrophoblast are homologous.

Linkages within the communities of invasive cells were driven by the expression of genes demonstrated to regulate cell invasion, including proteases *ADAM19*, *MMP15*[40], and *PAPPA2*[41], *ANXA4*[42], *GPC1*[27], *PLAC8*[43], and *CNFN* (**Figure 2a**; **Suppl. Table 2**). *ANXA4*, *FSTL3*, *PAPPA2*, and

PTPRF were shared between guinea pig (Cp_iEPT), human (Hs_GC), and mouse (Mm_TGC-SpA) extraplacental cells. Mouse invasive giant cells fell into a Euarchontoglires-specific SAMap community which included guinea pig invasive syncytiotrophoblast and human extravillous trophoblast (**Figure 2d**). SAMap linkages within this group were driven by expression of *FLT1*, *PTPRF*, *SEMA4C*, *SERPIN* and *PAPPA* family genes (**Suppl. Table 2**). Opossum SCT expressed only a few of the invasion-associated genes (*ADAM19*, *ANXA4*, and *ARID3A*; **Figure 2a**). Membership of Md_SCT-GCM1 in the Extraplacental I community was maintained in 93% of Leiden iterations; in the remaining 7%, it grouped instead with the Cytotrophoblast III community (**Figure 2d**), suggesting that its affinity to invasive cells was less robust. The presence of one invasive community with high species diversity and another restricted to Euarchtongolires could indicate that the diversity of invasive trophoblast populations in humans and rodents derive from an ancestral cell type related to the opossum syncytiotrophoblast. The latter hypothesis is attractive as the opossum syncytiotrophoblast is also the fetal cell population that is in direct contact with maternal tissues and has invasive properties[17].

In contrast, other phenotypic attributes of trophoblast, such as fusion and endoreduplication, did not form consistent SAMap communities suggestive of conserved transcriptomic identity (**Figure 2d**). Human syncytiotrophoblast had strong mapping to mouse spongiotrophoblast, but this association was driven by *Psg* and *Ceacam* family genes, which expanded independently in rodents and primates[44] and thus are not indicative of homology. While giant opossum knot cells (Md_SCG-GCM1) are histologically syncytial, their gene expression differed from other therian trophoblasts by inflammatory and growth factor production, and likewise guinea pig SCT clustered with other invasive cell types. We conclude that beyond short phylogenetic distances, homologies between syncytial trophoblasts or giant trophoblasts are unlikely, and instead have independent evolutionary origin.

The taxonomic distribution of cell populations in different putative homology groups suggests rapid evolution of functional phenotypes within families of homologous cells. The opossum had two trophoblast cell types (Md_SCT-GCM1 and Md_CTB) for which homology with trophoblast of eutherians was established. We interpret this as indicating that trophoblast cell types are evolutionarily descended from two ancestral trophoblast cell types which were present in the therian common ancestor. Furthermore, while the human and rodents both possess a diversity of interstitially and endovascularly invasive trophoblast cell types, in tenrec and opossum we find only a single invasive cell type. We conclude that the diversity of eutherian invasive trophoblasts descend from a single mononuclear cell type in the eutherian common ancestor which is retained in *Tenrec*. In boreoeutherian mammals, the greater diversity of invasive EPT cell types and acquisition of a conserved suite of invasion-associated genes suggest that this ancestral invasive potential was elaborated to give rise to a diversity of interstitially migratory and vascular remodeling cells.

Stepwise evolution of the uterine decidua in Eutheria

Decidualization is a coordinated tissue remodeling of the maternal endometrium during pregnancy, histologically apparent only in eutherian mammals in species with hemochorial placentation[45,46]. The decidual tissue's function is to regulate inflammation and fetal trophoblast invasion. The molecular mechanisms of decidual development are poorly known outside of humans and mice, but its cardinal cell type, the decidual stromal cell, exhibits gene-regulatory properties shared among eutherian mammals and lacking in the opossum and other marsupials[47,48]. Here, we used single-cell transcriptomes from our atlas to investigate whether the eutherian decidual stromal cell is a unitary cell type and whether there exists a gene-regulatory signature of decidual stromal cells conserved across mammalian species.

Recent single-cell studies[4,49] suggest greater human decidual diversity than the single canonical prolactin-producing cell type[45], which we refer to as endocrine decidua. We used matrix factorization to identify different co-regulated gene sets within the human endometrial stroma, agnostic of cell type annotations by the original authors: this process identified three decidual gene expression modules which roughly correspond to the three annotated decidual cell populations[4] (**Suppl. Figure 2; Suppl. Table 4**). The gene expression module of "Type I" decidual cells (Hs_dS1) included contractility- and myofibroblast-related genes including *ACTA2* and *TAGLN*, myosin light chain kinase *MYLK*, and

IGF1. This cell population was identified as a transient state during *in vitro* decidual cell differentiation[50]. The "Type II" (Hs_dS2) gene expression module included *HAND2, IL15, MEIS1, FOXO1*, *LEFTY2*, and *ADAMTS2* - genes upregulated during the initial wave of human in vitro decidualization[51] and commonly called "predecidual"[52] - and receptors *ESR1*, *PRLR*, and *INSR*. The human "Type III" (Hs_dS3) gene expression program included markers of mature endocrine decidua, *IGFBP1* and *PRL*[45], as well as *WNT4*, *PRSS23*, *MMP2*, and the decidual proteoglycans *DCN* and *LUM*.

In the opossum, two distinct stromal cell populations were present. These cells shared expression of *FOXO1*, *HOXA11*, estrogen receptor *ESR1* and progesterone receptor *PGR*. One population which we identified as endometrial stromal fibroblasts (Md_ESF-SMOC2) was enriched for *SMOC2*, *WNT5A*, and the relaxin receptor *RXFP1* (**Figure 3a**). We previously localized these cells to the stroma surrounding the opossum's endometrial glands[47]. We also found a population of *FBLN1*$^+$ fibroblasts (Md_TF-FBLN1) enriched for *CLEC3B*, *MFAP4*, and collagens *COL11A1* and *COL14A1*. *FBLN1*$^+$ fibroblasts were only present in the myometrium (**Figure 3b**) and thus are likely tissue fibroblasts.

Among the Md_ESF-SMOC2 cells, a number of *HAND2*$^+$ *IL15*$^+$ cells were detected in the opossum, similar in this respect to human dS2 "pre-decidual" cells. These cells comprised 29% of the *SMOC2*$^+$ population, but did not form a coherent population with sub-clustering, suggesting that all or most Md_ESF-SMOC2 cells may be able to express *IL15* and *HAND2* at very low levels. Uterine expression of *HAND2* and *IL15* was recently suggested as a synapomorphy of placental mammals and proposed as a first step towards assembly of the uterine decidua[53]. Our evidence suggests that *HAND2*$^+$ *IL15*$^+$ stromal cells are a developmentally accessible gene-regulatory state even for opossum ESC, but was stabilized into a robust cell type identity only later during eutherian evolution.

In the tenrec, three types of endometrial stromal cells were identified, united by expression of *HOXA11* and *HOXA9* (**Figure 3a**). HOXA11$^+$ cells were localized to the peri-glandular endometrial stroma (**Figure 3b**), like the opossum's Md_ESF-SMOC2 cells. Two of the three clusters, which together made up the majority (98%) of stromal cells, formed an inferred developmental trajectory from more fibroblast-like (Te_ESF) to more predecidual-like (Te_DSC-IL15) cells (**Figure 3c**). RNA velocity[54] analysis identified that the source of this trajectory consisted of cells enriched in *CLEC3B***,** *COL14A1*, *C7*, angiotensin *AGT*, and *SMOC2*, whereas more terminal cells express hormone receptors *ERBB4*, *RXFP1*, *ESR1* and *PGR*, decidual transcription factors *FOXO1*, *HAND2, and KLF7*, and *IL15*. IL15 is chemokine for uterine NK cells[55]. Unlike in the opossum, a large number of uterine NK cells were identified at the tenrec fetal-maternal interface (**Figure 1c**) which express a receptor for IL15 (*IL2RB+IL2RG*). The closest to a mature decidua in the tenrec was a small cluster representing 2% of stromal cells that were distinguished by the expression of cadherin *CDH2*, *WFDC1* and *CD9*. However, these cells were disconnected from Te_ESF and Te_DSC-IL15 in the UMAP embedding and instead grouped with pericytes, sharing expression of pericyte markers such as *RGS5* and *TBX3* but lacking the pericyte and endothelial-exclusive *MCAM*. Multipotential mesenchymal cells sharing markers of both pericytes and endometrial stromal fibroblasts have been described in the human[56]: the tenrec may share this source of endometrial stromal differentiation. Overall, the discovery of an *IL15*$^+$ *HAND2*$^+$ decidual cell population in *Tenrec ecaudatus* resembling *IL15*$^+$ human predecidual cells up to 29 days into gestation and lack of a clear endocrine decidual cell suggests that in this member of the basally divergent mammalian clade Afrotheria, the stroma persists in a state similar to the human predecidual cells.

The guinea pig stroma contained one ECM-remodeling and two endocrinologically active decidual cell populations. All three shared expression of *HOXA11*, *HOXA9*, *HAND2*, proteoglycans *DES* and *LUM*, *PGR* and *ESR1*, and rodent decidual marker *HOPX*[57] **(Figure 3a)**. The endocrine decidua included one cluster enriched in oxytocin *OXT* (Cp_gDSC-OXT), *PENK*, and the integrin *ITGA2*, and a cell population (Cp_DSC-PRL) expressing *prolactin*. These *PRL*$^+$ cells were larger and close to maternal spiral arteries (**Figure 3b**). The majority (84%) of stromal cells were marked by expression of *SMOC1*, *SMOC2*, *WNT2*, *WNT5A*, and hedgehog pathway genes *SMO* and *GLI3*. These *SMOC1*$^+$ cells are likely polyploid based on their size (**Figure 3b**) and expression of the cell cycle gene *E2F8* implicated in endoreduplication[58]. We identified them as giant decidual cells (Cp_gDSC-SMOC1) in line with previous descriptions[11], and localized SMOC1 staining to cells interspersed in

necrotic areas between the subplacenta and the decidua proper (**Figure 3b**). Decidual necrosis was also observed histologically (**Suppl. Figure 3**), presumably arising from the giant decidual cells[11].

The mouse decidua consisted of a single endocrine cell type (Mm_DSC) identified by the expression of the decidual prolactin paralog *Prl8a2* alongside *Pgr*, *Esr1*, *Hand2*, *Ctla2b*, and *Itgb3*. Additionally, a co-regulated set of 6 genes recently discovered to have maternally-biased parent-of-origin imprinting[59] - *Adamts5*, *Erv3*, *Mfap5*, *Tfpi2*, *Tnfrsf11b*, and *Tnfrsf23* - were specifically expressed (**Figure 3a**): these genes function in tumor suppression and may represent maternal mechanisms to regulate trophoblast invasion[60,61]. A subpopulation of decidual cells had reduced expression of *Pgr*, *Esr1*, *Hand2*, and *Hoxa11* but maintained expression of stress-related genes, including the chaperone *Cryab*, the inflammatory enzyme *Ctsk*, and the oxidative stress-related gene *Gpx3*. These we considered senescent decidua (Mm_snDSC), by analogy to progesterone-resistant senescent decidual cells identified in the human[52]. Cells corresponding to the predecidual cells in tenrec and human were absent, but a fibroblast population (Mm_acTF) with an ECM-remodeling transcriptomic signature was identified. This cell type expressed fibroblast activation protein *Fap*, collagens, *Clec3b* and *Mfap4*, as well as the hedgehog genes *Gli3*, *Ptch1*, and *Smo*, but lacked expression of sex steroid receptors, and thus was likely a generic tissue fibroblast.

Assessing the evolutionary history of decidual cell types

While the cell type phylogeny (**Figure 1e**) identified high-level family groupings, it did not resolve decidual cell type relationships to the degree necessary to make confident statements about homology across species. To address fine-scale decidual cell type relationships, we compared species using transcriptomic similarity (SAMap community detection) as well as identification gene co-regulatory modules (cNMF).

Network analysis of SAMap mapping scores identified two communities of endometrial stromal cell types, one consisting of more mature decidual cell types and the other of ECM-depositing and predecidual stromal cells (**Figure 3d**). The more decidualized community included the two endocrine decidua of the guinea pig (*OXT*$^+$ and *PRL*$^+$), mouse Mm_DSC and Mm_snDSC, human Hs_dS2, and tenrec Te_DSC-CDH2. The less decidualized stromal cell community consisted of the opossum *SMOC2*$^+$ and *FBLN1*$^+$ fibroblasts, tenrec ESF and *IL15*$^+$ decidual cells, guinea pig giant *SMOC1*$^+$ DSC, mouse tissue fibroblasts and the human dS1 cell population. The inclusion of tissue fibroblasts and *Monodelphis* endometrial fibroblasts shows that the decidual cells in this community are less specialized than the cells in the previous community.

Both decidua-like communities showed a clear distinction with respect to other mesenchymal cell types, smooth muscle cells and fetal fibroblasts (**Figure 3d**). Mapping scores of ECM-depositing and decidual stroma subsets were analyzed in more detail (**Figure 3e**). Prolactin-expressing decidua of the mouse (Mm_DSC) and guinea pig (Cp_DSC-PRL) mapped strongly to one another, with driving genes including *PGR*, *ESR1*, *VIM*, *DES*, *LUM*, *SERPING*, *ITGB*, *HAND2*, and *HOXA11*, suggesting homology of what we call *endocrine decidua* in mouse and guinea pig. The human *PRL*$^+$ decidual cluster (Hs_dS3) had comparatively weak mapping to decidual cells of other species. This may be explained by lineage-specific evolutionary modifications to the human decidual stromal cell type, including spontaneous decidualization. Human predecidual Hs_dS2, instead, mapped to decidua from other mammals most broadly. *IL15*$^+$ stromal cells from the tenrec, guinea pig *SMOC1*$^+$ stroma, and opossum *SMOC2*$^+$ stroma mapped to each other, supporting the notion that the tenrec possesses a persistent predecidual phenotype which, given its similarity to opossum stroma, is likely a more primitive decidual state.

We next looked for cross-species conservation of gene co-regulation in decidual cells (**Suppl. Figure 2**). A hierarchically-clustered correlation matrix of gene loadings (**Figure 3f**) identified two families of gene regulatory programs - a broad therian endometrial and predecidual gene regulatory state, and an eutherian-specific grouping of gene expression modules which included those expressed in endocrine decidua (**Figure 3f**). Among the predecidual modules, the human Hs_dS2 gene module was most similar to gene modules discovered in Te_DSC-IL15 and in Cp_gDSC-SMOC1 cells. The predecidual-like programs were united by high loadings of *MEIS1*, *WT1*, *ESR1*, *PGR*, and *EGFR*

(**Suppl. Figure 8**). Gene expression modules expressed in endocrine decidua of human, mouse, and guinea pig, as well as tenrec *CDH2*$^{+}$ stroma, grouped together (**Figure 3f**). Their similarity was driven mostly by *LUM* and *DCN*, *VIM*, *PPIB*, and *DUSP1* (**Suppl. Table 4**), and no counterpart was identified in the opossum. Negative correlation was detected between the predecidual and the undifferentiated or mature decidual (Type I and Type III) gene expression programs in tenrec, guinea pig, and human (**Figure 3f**), and genes in the predecidual-like cells tended to be expressed in different cells than the mature decidua (**Suppl. Figure 8**). We interpret this as evidence that eutherian mammals exhibit a unique division of gene-regulatory functions into two reciprocally antagonistic gene regulatory states: one active in endocrine and the other in the non-endocrine endometrial stromal cells.

Integrating these forms of evidence leads to the following model for the evolution of the uterine decidual cells (**Figure 3h**). On one hand, there are cells with strong affinity to matrix-remodeling and undifferentiated endometrial fibroblasts which we call Type I cells. Eutherians share a division between two decidual cell type families: the predecidual or "Type II" decidual cells and endocrine decidual cells, or "Type III". This division is supported by the negative correlation between co-regulated gene modules of the two cell types (**Figure 3f**). "Type II" decidual cells are likely modified from the ancestral therian stroma by upregulation of *IL15* expression via *HAND2*, as identified by comparative transcriptomics[62]. In the two rodents sampled, no mesenchymal cell type produces *IL15*; instead, decidual *IL15* is solely produced by macrophages. However, the deep phylogenetic age of the tenrec-human divergence suggests that in the rodent lineage *IL15* production was shifted from decidual fibroblasts to decidual macrophages. The endocrine decidual cell type family unites cells from tenrec, guinea pig and mouse. Human "Type III" *PRL*$^{+}$ decidua show weak affinity to *PRL*$^{+}$ cells in rodents and instead group with more fibroblast-like Type I cells from opossum and tenrec. This may reflect their independent evolutionary derivation from an ancestral cell type[63] after the rodent-primate divergence, or may be due to the evolution of spontaneous decidualization in the primate lineage. Prolactin production, used as an empirical proxy for human and mouse decidualization[45], is not an identity-defining characteristic of the decidual stromal cell, but rather a "plug-in" which was added to an ancestral Type I-like stroma in the case of primates, or a Type II-like stromal cell in the case of rodents. In these two lineages, decidual PRL expression is driven by independently evolved alternative promoters[64]. These findings suggest that decidual stromal cell diversity expanded within crown Placentalia in at least two steps, one with the establishment of the Type II identity, followed by the establishment of an endocrine decidual cell type, possibly independently in rodents and primates.

Co-evolutionary dynamics of cell communication

Hemochorial placentation unites two tissues – the fetal trophoblast and the maternal endometrium – and consequently creates a new physiological system. We asked to what degree fetal and maternal cell types showed evidence of a co-evolutionary history. We inferred signaling between cell types from complementary ligand-receptor gene expression and traced the co-evolutionary history of these interactions within Theria.

Invasive trophoblast cells are integrated into the endometrial signaling network

The evolution of a novel cell type is predicted to be followed by increasing functional integration with other cells in the tissue[65]. First, as an approximation of signaling integration, we asked whether there are systematic differences in the number of non-autocrine ("allocrine") interactions between cell types. Allocrine ligand and receptor counts were positively correlated (Pearson; $p < 0.05$ in all species except *Monodelphis*), suggesting a line between cells with low and high degrees of integration (**Figure 4a**). Stromal cells, including fibroblasts and eutherian decidual stromal cells, had the greatest degrees of allocrine signaling, indicating that they constitute a highly-connected signaling hub for both incoming and outgoing signals. Some trophoblast showed high proportions of allocrine signaling, including human and opossum cytotrophoblast, and the predominantly invasive trophoblasts (Hs_iEVT, Hs_eEVT, Te_EPT, Cp_EPT-CCC, Cp_EPT-OXT, Mm_TGC_Gly). We interpret this to mean that the cell types that make direct contact with maternal cells have evolved substantial signaling

integration with maternal cells. Macrophages and endothelial cells ranked intermediately, whereas syncytiotrophoblast and immune effector cells (BC, TC, NKC, PMN) showed the lowest proportions of allocrine receptors (**Figure 4a**). Indeed, trophoblast and decidual stromal cells were among the top signaling "hubs" (greatest outgoing signaling strength) according to additional graph statistics, with *Monodelphis GCM1+* trophoblast and human Type III decidua tied for the highest HITS hub scores among all cell types, and lymphoid cells from all species among the lowest (**Suppl. Figure 9**). The latter pattern may reflect the principle that peripheral immune cells do not inhabit a stable tissue niche and thus cannot evolve strong integration to a single tissue microenvironment[66].

Evidence for disambiguation of fetal and maternal signals

Evolutionary signaling theory predicts that maternal and fetal co-production of signals is selected against because a signal that emanates from the fetus and the mother does not identify the origin of the signal. As a consequence it is predicted that fetal-maternal signaling systems will evolve towards maternal-only or fetal-only expression to allow the mother to distinguish between herself and the fetus as a source[8]. Such a process would manifest as a disambiguation pattern, with ligand production restricted to fetal or maternal cell types, but not both. We compared the observed number of fetal-only and maternal-only expressed ligands from different signaling families (e.g. WNT, NOTCH) against a null statistical model (**Figure 4b; Suppl. Figure 10; Suppl. Table 5**: see **Methods**). In all species, fetal and maternal co-expression of ligands was lower than expected by our null model (**Figure 4b**, left panel). Significantly disambiguated pathways showed increased fetal-only and/or maternal-only expression of component members, with the most consistently disambiguated ligand and signal modulating gene families across species included WNT, steroids, FGFs, various families of immunomodulatory factors, and IGFBPs (**Figure 4b**).

Ligand family expansion through gene duplication has likely played a role in the evolution of disambiguation via the creation of novel placenta- or decidua-specific paralogs. In rodents, the *prolactin* gene family includes 26 paralogs in the mouse and 10 in the guinea pig, whereas in primates, a different somatotropin, *growth hormone*, has duplicated leading to the origin of the placentally expressed *CSH1*, *CSH2*, and *GH2*. Mouse *prolactin* genes showed a strongly disambiguated expression pattern, with 10 exclusively fetal paralogs, 10 ambiguous paralogs (fetal and maternal co-expression), and zero exclusively maternal paralogs (**Suppl. Table 6**). The human showed moderate somatotropin disambiguation: *GH2* was fetal-only, *CSH1* and *CSH2* were ambiguous, and *PRL* was maternal-only. Cell type-specific growth factors involved in core tissue homeostasis, such as *VEGF*, *PDGF*, and *CSF1*, on the other hand, showed an overwhelmingly bilateral/ambiguous expression, likely with local signaling reach (**Suppl. Table 5**).

In the opossum, extreme production by the trophoblast of the angiogenic factor *VEGFA* can be interpreted as a nutrient-soliciting signal. If this is the case, the disambiguation model [8] predicts that in an evolutionary stable state, the mother should silence her own copy or utilize a different VEGF paralog. However, we found no fetal-specific vascular endothelial growth factor paralog in the opossum. This lack of disambiguation may be explained by developmental constraint, due to the role of VEGF in tissue homeostasis countervailing the selection for disambiguation. Alternatively, disambiguation may be achieved by maternal utilization of a splice variant of VEGFA with differential signaling properties, as documented with the $VEGF_{111}$ isoform in the marsupial *Sminthopsis crassicaudata*, the rat, and viviparous skinks[67].

Primates and rodents show accelerated evolution of signaling interactions

We examined the branches along which interactions arose or were lostusing ancestral state reconstruction. To resolve homology of sending and receiving cell types across species, we grouped cell types by fetal or maternal origin (character states in **Suppl. Table 7**) and according to the broad families from the cell tree (character states in **Suppl. Table 8**). Maximum-parsimony ancestral states reconstruction of fetal-to-maternal secreted signals identified 135 signals which the placenta of the first viviparous mammal, i.e., the common ancestor of *Theria*, can be inferred to have sent to the mother

(**Figure 4c**). These included relaxin *RLN2*, platelet-derived growth factors *PDGFA* and *PDGFC*, prostaglandin E2 via expression of *PTGES2* and *PTGES3*, and *TGFB1* and *TGFB2*. Of these, 49 were conserved in all 5 tip species.

Comparison of reconstructed states traced the gains and losses to this therian interaction set (**Figure 4c**). At the *Placentalia* node, we inferred the gain of an additional 90 signals, including the macrophage chemokine *CXCL12*, the vascular growth factor *VEGFB*, and the insulin-like growth factor *IGF2* (**Figure 4d**). Within placental mammals, human, mouse, and guinea pig belong to the clade Euarchontoglires; this stem lineage evolved 6 fetal-maternal signals absent in the basally branching *Tenrec*, including *CCL4* and *GDF11*. The two rodents in our taxon sample, *Cavia porcellus* and *Mus musculus*, shared an additional 11 interactions, including *EDN2*, *TGFA*, *CX3CL1*, and *prolactin*. Many fetal-to-maternal ligand-receptor interactions were species-specific. *Mus musculus* saw an expansion of novel *CEACAM* genes, and the guinea pig placenta was unique in *OXT* production, typically considered part of parturition. The human lineage saw the acquisition of novel *GH* paralogs. *Monodelphis domestica* contrasted with eutherians in the production of inflammatory cytokines, including *IL1A*, *IL6*, and *IL17A* which could reflect an ancestral therian state of inflammatory placentation[19] or an autapomorphy of the didelphid lineage, where the fetus contributes to producing the signals for parturition[68].

We calculated rates of evolutionary change in fetal-to-maternal signaling by tracing our reconstructed ancestral states on a time-calibrated mammalian tree[69]. The lineage leading to *Monodelphis domestica*, the stem Eutherian lineage, and the lineage leading to *Tenrec ecaudatus* showed slow turnover, fewer than 0.5 gains or losses per Myr, whereas in Euarchontoglires, rates of change were more than twice as high and up to 1.82 changes/Myr in the stem lineage of Euarchontoglires (**Figure 4c**), suggesting more rapid evolution of fetal-maternal communication in Boreoeutherians than in basally branching placentals and marsupials.

Escalation of fetal-maternal signaling is limited

A prediction for fetal-maternal signaling is the presence of an asymmetric evolutionary arms race[70] in which gains to fetal signaling strength are matched by reduced maternal responsiveness[9]. We tested for this pattern at the transcriptomic level by comparing reconstructed evolutionary changes in signal and cognate receptor mRNA expression across internal branches of our 5-species phylogenetic tree. However, when modeling ligand and receptor expression as binary on/off traits using expression thresholding, lineages in which more fetal ligands were gained saw more gains in maternal receptors, rather than losses (**Figure 4c**). We tested instead for a quantitative escalation pattern without complete suppression by modeling changes in expression levels as continuous traits. When considering all secreted signaling peptides or just those classified as growth factors (GO:0008083), inferred evolutionary changes along internal branches of the tree did not show overwhelming prevalence towards asymmetric changes in fetal and maternal expression (**Suppl. Figure 11**). These findings suggest that placental-maternal signaling gene expression does not follow an exclusively antagonistic dynamic. Such a dynamic may be realized at the post-transcriptional level, as in the case of decoy receptors[71], or in the chemical properties of signal peptides such as half-life[72] which cannot be inferred from mRNA expression.

Eutherians integrate lymphoid cells into the decidual signaling network

A particular form of co-evolved integration between cell types crucial for tissue homeostasis is growth factor signaling[73]. To test whether cells at the fetal-maternal interface regulate each others' growth in this way, we examined the patterns of reciprocal growth factor signaling between cell type homology groups. We used a data-driven approach to quantify cell type-specificity of growth factors. We calculated Gini coefficients of in-degree distributions for each growth factor's cell-cell signaling network (see **Methods**). The Gini coefficient measures the inequality of the distribution of a random variable. Growth factors such as IGF1, IGF2, and TGFB1 exhibited the lowest scores, indicating widespread connectivity (**Suppl. Figure 12**). Cell type-specific growth factors (Gini coefficient ≥ 0.8),

are more likely to represent specific signaling relationships between cell types, as opposed to broadcast endocrine signals. Examples are VEGF and PDGF which displayed high target cell type specificity. We used cycle detection[74] to identify cells linked by reciprocal signaling. We found, across the four eutherian species, reciprocal cell type-specific growth factor signaling existed among all of the major uterine cell classes (**Figure 4e; Suppl. Figure 13**). In the opossum, however, maternal lymphoid cells did not produce growth factors for other maternal or fetal cells. Opossum uterine lymphoid cells differed from those of eutherians in that they consisted of only T and B cells, but lacked NK cells. In eutherians the integration of lymphoid cells into the endometrial signaling network is mostly due to the role of uterine natural killer cells. This suggests that a significant alteration in cell growth regulatory dynamics resulted from the origination of tissue-specific lymphoid cells (uNK) in the eutherian decidua.

Discussion

The fetal-maternal interface is the product of at least three major evolutionary events. The origin of a direct contact between extraembryonic and maternal tissues in therian mammals created a new avenue for nutrient exchange and communication[75]. A second key innovation of placental mammals was the decidua, likely necessary for enabling sustained placental implantation[17]. The third innovation was invasive trophoblast, a cell type elaborated in eutherians[2] and reaching an extreme in species with deep invasion such as humans and guinea pigs. In this manuscript, we described the cell type composition and cell-cell ligand-receptor signaling of species spanning these transitions to identify how evolution at the cellular level relates to these changes at higher levels of organization.

Using a combination of phylogenetic and pairwise mapping, we investigated placental and decidual cell type homology across species. Our results suggest that eutherians underwent an expansion in trophoblast cell type diversity. We infer that the therian ancestor, like the extant opossum, had two trophoblast cell types, one putatively homologous to eutherian cytotrophoblast, and the other specialized in signaling to the mother with weak invasive potential. Invasive extraplacental trophoblast of tenrec, guinea pig and human and spiral artery-remodeling trophoblast in the mouse shared a common gene signature suggestive of homology. The presence of a putative homolog to human extravillous trophoblast in the basally-branching *Tenrec*, and the reciprocal linkage of trophoblast transcriptomes by invasive potential, suggest that the invasive/noninvasive phenotypic divide may reflect an ancient divide in trophoblast cell type identity. The diversity of the invasive trophoblast cell types further expanded within Euarchontoglires, generating interstitial and endovascular sub-types.

In the endometrial stroma, we identified a more diverse family of decidual stromal cells than previously recognized. The discovery of a primitive predecidual cell in *Tenrec ecaudatus*, with broad conservation across eutherians, suggests that decidual cells evolved by at least two cell type origination events. One early in the eutherian history leading to the origin of immunomodulatory ($IL15^{+}$) predecidual cells. The acquisition of endocrine signaling capabilities by decidual stromal cells appears to have occurred later in eutherian evolution.

Cell type evolution at the fetal-maternal interface shows evidence of parallel evolution. Therian syncytiotrophoblasts are transcriptomically heterogenous, which we interpret as indicating origins from different ancestral cell types (**Figure 2d**). In addition these cells perform different functions - from inflammatory and growth factor signaling in opossum, invasion in guinea pig, vascular interface in mouse, to gonadotropin production in the human. Likewise, while prolactin-producing endocrine decidua in rodents show high transcriptpomic similarity, neither showed high similarity to prolactogenic human Type III decidual cells. Molecular evidence suggests that decidual prolactin expression evolved by independent transposable element insertions upstream of the *prolactin* promoters in rodents and primates[64], and likewise, independent events of retroviral insertion led to the origin of fusogenic *syncytin* genes in all five mammalian lineages in our study[76–78]. These findings suggest that trophoblast and decidual evolution has involved parallel evolution of cell phenotypes - fusion, hormone production - by recruitment of retroviral elements into gene regulatory networks of non-homologous ancestral cell types.

Compelling theoretical models have long been advanced about the co-evolutionary signaling dynamics between the fetus and mother[9]. Here we use transcriptome-wide data to test some of these predictions. Our test of the disambiguation hypothesis[8] revealed consistent and strong overrepresentation of both fetal-specific and maternal-specific ligand repertoires. This pattern was driven in part by recent gene duplication into fetal-specific paralogs as with *prolactin* and *Psg* gene family expansion in the mouse lineage[44]. A logical next step would be to investigate genetic mechanisms driving disambiguation, for instance capture of ligand genes by fetal-specific enhancers[79]. Another prediction of conflict theory, the escalation hypothesis, predicts that increased fetal ligand production would be complemented by reduction in corresponding receptor expression by the mother. However, we did not find this pattern in our data; instead, gains in ligands were complemented by gains in receptors. Finally, we used ancestral state reconstruction to trace the history of ligand-receptor signaling co-evolution, recovering the shared cell signaling interactions of the Placental common ancestor, and found that Boreoeutherians underwent a more rapid divergence in fetal-maternal signaling than the opossum and tenrec lineages.

We acknowledge limitations to the inference of ligand-receptor signaling from RNA expression. The potential for false negatives due to sequencing drop-out, incomplete genome annotation in non-model species, and protein-protein interaction divergence likely inflate the number of lineage-specific signaling innovations our phylogenetic analysis infers. We restricted analysis to secreted ligands, as interactions mediated by cell-cell contact require spatial information to judge their plausibility. Spatially-resolved RNA sequencing would be able to examine interactions of this kind.

The evolutionary approach we introduce for cell-cell communication holds potential for broader applications across various systems. This methodology offers a gateway to uncover the co-evolution of cell types within a tissue, and opens avenues for exploring multi-species symbioses, exemplified by recent advances in single-cell transcriptomics of multicellular parasites[80] and commensals[81].

The fetal-maternal interface has attracted attention in recent years as a model system for single-cell genomics and ligand-mediated cell signaling at scale[4,5]. The next research frontier in single-cell reproductive biology entails comparing cell types across species to uncover the origins of phenotypic diversity and trace cell type evolution. The multi-species atlases we present here demonstrate that the field has reached the point where long-standing evolutionary questions about parent-offspring coevolution and biological tissue organization can be addressed at a resolution heretofore impossible. Our results reveal a diversity of cell types whose phylogenetic history will require more extensive sampling to completely untangle. Unanswered questions include the molecular genetic mechanisms behind observed patterns of signaling integration and disambiguation. Nevertheless, the outlines of a multistage history of increasing cell type and communicative complexity can now be seen. As high-throughput genomics of non-traditional model species becomes more technologically accessible, expanded taxon sampling will allow the kinds of phylogenetic reconstructions we introduce here to expand in precision and scope.

Data Availability

Sequencing data will be uploaded to NCBI Gene Expression Omnibus.

End Notes

The research presented was supported by the Yale Institute for Biospheric Studies, the John Templeton Foundation (#61329), the National Science Foundation (NSF IOS 1655091) and the Austrian Science Fund (FWF 33540). D.J.S. was supported by the NIH (T32 GM 007499) and D.J.S. and S.B. were supported by the NSF g2p2pop Research Coordination Network (RCN 1656063). The Yale Center for Genomic Analysis (NIH 1S10OD030363-01A1) and Yale West Campus Imaging Core supported this work. G.P.W. receives research support from the Hagler Institute of Advanced Studies at Texas A&M University. The authors thank Katie Grabek of Fauna Bio, Michael Hiller and Evgeny Leushkin for sharing the draft *Tenrec ecaudatus* genome. The study benefited from input from

members of the Pavlicev and Wagner labs. Steve Stearns and Arun Chavan provided critical comments on the manuscript.

Author Contributions

D.J.S, S.B., G.P.W., and M.P. designed the study. G.P.W., M.P., F.vB., D.J.S. and S.B. secured funding. D.J.S., S.B., J.D.M., A.G.C. and G.P.W. conducted experiments. G.R.S., G.D., J.D.M., D.J.S. and S.B. maintained animal colonies. D.J.S. and S.B. conducted analysis. D.J.S. and S.B. drafted the manuscript. G.P.W. and M.P. edited the manuscript. All authors provided comments and approved the manuscript before submission.

References

1. Mess, A. & Carter, A. M. Evolutionary transformations of fetal membrane characters in Eutheria with special reference to Afrotheria. *J. Exp. Zoolog. B Mol. Dev. Evol.* **306B**, 140–163 (2006).
2. Wildman, D. E. *et al.* Evolution of the mammalian placenta revealed by phylogenetic analysis. *Proc. Natl. Acad. Sci.* **103**, 3203–3208 (2006).
3. Pavličev, M. *et al.* Single-cell transcriptomics of the human placenta: inferring the cell communication network of the maternal-fetal interface. *Genome Res.* **27**, 349–361 (2017).
4. Vento-Tormo, R. *et al.* Single-cell reconstruction of the early maternal–fetal interface in humans. *Nature* **563**, 347–353 (2018).
5. Arutyunyan, A. *et al.* Spatial multiomics map of trophoblast development in early pregnancy. *Nature* **616**, 143–151 (2023).
6. Grosser, O. Die Placenta von Centetes und ihre Lehren betreffs der Stoffaufnahme in den Placenten. *Z. Für Anat. Entwicklungsgeschichte* **88**, 509–521 (1928).
7. Strahl, H. Beiräge zur vergleichenden Anatomie der Placenta. *Abhandl Senckenberg Naturf Gesell* **27**, 263–319 (1905).
8. Haig, D. Placental hormones, genomic imprinting, and maternal—fetal communication. *J. Evol. Biol.* **9**, 357–380 (1996).
9. Haig, D. Genetic conflicts in human pregnancy. *Q. Rev. Biol.* **68**, 495–532 (1993).
10. Kotliar, D. *et al.* Identifying gene expression programs of cell-type identity and cellular activity with single-cell RNA-Seq. *eLife* **8**, e43803 (2019).
11. Davies, J., Dempsey, E. W. & Amoroso, E. C. The subplacenta of the guinea-pig: development,

histology and histochemistry. *J. Anat.* **95**, 457–473 (1961).

12. Tarashansky, A. J. *et al.* Mapping single-cell atlases throughout Metazoa unravels cell type evolution. *eLife* **10**, e66747 (2021).

13. Arendt, D. *et al.* The origin and evolution of cell types. *Nat. Rev. Genet.* **17**, 744–757 (2016).

14. Bischof, P. & Irminger-Finger, I. The human cytotrophoblastic cell, a mononuclear chameleon. *Int. J. Biochem. Cell Biol.* **37**, 1–16 (2005).

15. Zhao, Y. *et al.* Rapid structural change in synaptosomal-associated protein 25 (SNAP25) precedes the fusion of single vesicles with the plasma membrane in live chromaffin cells. *Proc. Natl. Acad. Sci.* **110**, 14249–14254 (2013).

16. Papuchova, H. & Latos, P. A. Transcription factor networks in trophoblast development. *Cell. Mol. Life Sci.* **79**, 337 (2022).

17. Chavan, A. R. *et al.* Evolution of Embryo Implantation Was Enabled by the Origin of Decidual Stromal Cells in Eutherian Mammals. *Mol. Biol. Evol.* **38**, 1060–1074 (2021).

18. Zeller & Freyer. Early ontogeny and placentation of the grey short-tailed opossum, Monodelphis domestica (Didelphidae: Marsupialia): contribution to the reconstruction of the marsupial morphotype. *J. Zool. Syst. Evol. Res.* **39**, 137–158 (2001).

19. Griffith, O. W. *et al.* Embryo implantation evolved from an ancestral inflammatory attachment reaction. *Proc. Natl. Acad. Sci.* **114**, E6566–E6575 (2017).

20. Hansen, V. L., Faber, L. S., Salehpoor, A. A. & Miller, R. D. A pronounced uterine pro-inflammatory response at parturition is an ancient feature in mammals. *Proc. R. Soc. B Biol. Sci.* **284**, 20171694 (2017).

21. Zhu, Y.-N. *et al.* The Role of DNMT1 and C/EBPα in the Regulation of CYP11A1 Expression During Syncytialization of Human Placental Trophoblasts. *Endocrinology* **165**, bqad195 (2024).

22. Carter, A. M. Evolution of Placental Function in Mammals: The Molecular Basis of Gas and Nutrient Transfer, Hormone Secretion, and Immune Responses. *Physiol. Rev.* **92**, 1543–1576 (2012).

23. Brandt, D. T. *et al.* SCAI acts as a suppressor of cancer cell invasion through the transcriptional control of β1-integrin. *Nat. Cell Biol.* **11**, 557–568 (2009).

24. Yang, X. & Meng, T. MicroRNA-431 affects trophoblast migration and invasion by targeting ZEB1 in preeclampsia. *Gene* **683**, 225–232 (2019).

25. Carter, A. M., Blankenship, T. N., Künzle, H. & Enders, A. C. Development of the haemophagous region and labyrinth of the placenta of the tenrec, Echinops telfairi. *Placenta* **26**, 251–261 (2005).

26. Scott, R. L. *et al.* Conservation at the uterine–placental interface. *Proc. Natl. Acad. Sci.* **119**, e2210633119 (2022).

27. Aikawa, T. *et al.* Glypican-1 modulates the angiogenic and metastatic potential of human and mouse cancer cells. *J. Clin. Invest.* **118**, 89–99 (2008).

28. Zadora, J. *et al.* Disturbed Placental Imprinting in Preeclampsia Leads to Altered Expression of DLX5, a Human-Specific Early Trophoblast Marker. *Circulation* **136**, 1824–1839 (2017).

29. Mess, A., Zaki, N., Kadyrov, M., Korr, H. & Kaufmann, P. Caviomorph Placentation as a Model for Trophoblast Invasion. *Placenta* **28**, 1234–1238 (2007).

30. Weiler, P., Lange, M., Klein, M., Pe'er, D. & Theis, F. J. Unified fate mapping in multiview single-cell data. 2023.07.19.549685 Preprint at https://doi.org/10.1101/2023.07.19.549685 (2023).

31. Alam, S. M. K. *et al.* Prolactin Family of the Guinea Pig, Cavia porcellus. *Endocrinology* **151**, 3918–3928 (2010).

32. Marsh, B. & Blelloch, R. Single nuclei RNA-seq of mouse placental labyrinth development. *eLife* **9**, e60266 (2020).

33. Han, X. *et al.* Mapping the Mouse Cell Atlas by Microwell-Seq. *Cell* **172**, 1091-1107.e17 (2018).

34. Simmons, D. G. *et al.* Early patterning of the chorion leads to the trilaminar trophoblast cell structure in the placental labyrinth. *Development* **135**, 2083–2091 (2008).

35. Simmons, D. G., Rawn, S., Davies, A., Hughes, M. & Cross, J. C. Spatial and temporal expression of the 23 murine Prolactin/Placental Lactogen-related genes is not associated with their position in the locus. *BMC Genomics* **9**, 352 (2008).

36. Tunster, S. J., Watson, E. D., Fowden, A. L. & Burton, G. J. Placental glycogen stores and fetal

growth: insights from genetic mouse models. *Reproduction* **159**, R213–R235 (2020).

37. Zhang, Q., Hao, J. & Li, G. Deletion of Prl7d1 causes placental defects at mid-pregnancy in mice. *Mol. Reprod. Dev.* **86**, 696–713 (2019).

38. Cindrova-Davies, T. *et al.* RNA-seq reveals conservation of function among the yolk sacs of human, mouse, and chicken. *Proc. Natl. Acad. Sci.* **114**, E4753–E4761 (2017).

39. Ohgushi, M., Taniyama, N., Vandenbon, A. & Eiraku, M. Delamination of trophoblast-like syncytia from the amniotic ectodermal analogue in human primed embryonic stem cell-based differentiation model. *Cell Rep.* **39**, 110973 (2022).

40. Zhao, M., Qiu, W., Li, Y., Sang, Q. A. & Wang, Y. Dynamic change of Adamalysin 19 (ADAM19) in human placentas and its effects on cell invasion and adhesion in human trophoblastic cells. *Sci. China C Life Sci.* **52**, 710–718 (2009).

41. Chen, X. *et al.* The potential role of pregnancy-associated plasma protein-A2 in angiogenesis and development of preeclampsia. *Hypertens. Res.* **42**, 970–980 (2019).

42. Xu, Y. *et al.* ANXA4 promotes trophoblast invasion via the PI3K/Akt/eNOS pathway in preeclampsia. *Am. J. Physiol.-Cell Physiol.* **316**, C481–C491 (2019).

43. Chang, W.-L. *et al.* PLAC8, a new marker for human interstitial extravillous trophoblast cells, promotes their invasion and migration. *Development* **145**, dev148932 (2018).

44. Kammerer, R. & Zimmermann, W. Two waves of evolution in the rodent pregnancy-specific glycoprotein (Psg) gene family lead to structurally diverse PSGs. *BMC Genomics* **24**, 468 (2023).

45. Gellersen, B. & Brosens, J. J. Cyclic Decidualization of the Human Endometrium in Reproductive Health and Failure. *Endocr. Rev.* **35**, 851–905 (2014).

46. Critchley, H. O. D. *et al.* Menstruation: science and society. *Am. J. Obstet. Gynecol.* **223**, 624–664 (2020).

47. Kin, K., Maziarz, J. & Wagner, G. P. Immunohistological Study of the Endometrial Stromal Fibroblasts in the Opossum, Monodelphis domestica: Evidence for Homology with Eutherian Stromal Fibroblasts1. *Biol. Reprod.* **90**, (2014).

48. Brayer, K. J., Lynch, V. J. & Wagner, G. P. Evolution of a derived protein–protein interaction

between HoxA11 and Foxo1a in mammals caused by changes in intramolecular regulation. *Proc. Natl. Acad. Sci.* **108**, E414–E420 (2011).

49. Suryawanshi, H. *et al.* A single-cell survey of the human first-trimester placenta and decidua. *Sci. Adv.* **4**, eaau4788 (2018).

50. Stadtmauer, D. J. & Wagner, G. P. Single-cell analysis of prostaglandin E2-induced human decidual cell in vitro differentiation: a minimal ancestral deciduogenic signal. *Biol. Reprod.* (2021) doi:10.1093/biolre/ioab183.

51. Rytkönen, K. T. *et al.* Decidualization of Human Endometrial Stromal Fibroblasts is a Multiphasic Process Involving Distinct Transcriptional Programs. *Reprod. Sci.* **26**, 323–336 (2019).

52. Rawlings, T. M. *et al.* Modelling the impact of decidual senescence on embryo implantation in human endometrial assembloids. *eLife* **10**, e69603 (2021).

53. Mika, K., Whittington, C. M., McAllan, B. M. & Lynch, V. J. Gene expression phylogenies and ancestral transcriptome reconstruction resolves major transitions in the origins of pregnancy. *eLife* **11**, e74297 (2022).

54. Bergen, V., Lange, M., Peidli, S., Wolf, F. A. & Theis, F. J. Generalizing RNA velocity to transient cell states through dynamical modeling. *Nat. Biotechnol.* **38**, 1408–1414 (2020).

55. Erlebacher, A. Immunology of the maternal-fetal interface. *Annu. Rev. Immunol.* **31**, 387–411 (2013).

56. Spitzer, T. L. B. *et al.* Perivascular Human Endometrial Mesenchymal Stem Cells Express Pathways Relevant to Self-Renewal, Lineage Specification, and Functional Phenotype1. *Biol. Reprod.* **86**, 58, 1–16 (2012).

57. Li, R. *et al.* Spatial transcriptomic profiles of mouse uterine microenvironments at pregnancy day 7.5. *Biol. Reprod.* **107**, 529–545 (2022).

58. Qi, Q.-R. *et al.* Involvement of atypical transcription factor E2F8 in the polyploidization during mouse and human decidualization. *Cell Cycle* **14**, 1842–1858 (2015).

59. Rodriguez-Caro, F., Moore, E. C. & Good, J. M. Evolution of parent-of-origin effects on placental gene expression in house mice. 2023.08.24.554674 Preprint at

https://doi.org/10.1101/2023.08.24.554674 (2023).

60. Kumar, S., Sharghi-Namini, S., Rao, N. & Ge, R. ADAMTS5 Functions as an Anti-Angiogenic and Anti-Tumorigenic Protein Independent of Its Proteoglycanase Activity. *Am. J. Pathol.* **181**, 1056–1068 (2012).

61. Xiao, X. *et al.* Hypomethylation of tissue factor pathway inhibitor 2 in human placenta of preeclampsia. *Thromb. Res.* **152**, 7–13 (2017).

62. Mika, K. *et al.* Evolutionary transcriptomics implicates new genes and pathways in human pregnancy and adverse pregnancy outcomes. *eLife* **10**, e69584 (2021).

63. Wu, L., Stadtmauer, D. J., Maziarz, J. & Wagner, G. Decidual cell differentiation is evolutionarily derived from fibroblast activation. 2020.12.18.423527 Preprint at https://doi.org/10.1101/2020.12.18.423527 (2020).

64. Emera, D. *et al.* Convergent Evolution of Endometrial Prolactin Expression in Primates, Mice, and Elephants Through the Independent Recruitment of Transposable Elements. *Mol. Biol. Evol.* **29**, 239–247 (2012).

65. Griffith, O. W. & Wagner, G. P. The placenta as a model for understanding the origin and evolution of vertebrate organs. *Nat. Ecol. Evol.* **1**, 1–10 (2017).

66. Pavlicev, M. & Wagner, G. Reading the Palimpsest of Cell Interactions: What Questions May We Ask of the Data? *iScience* (2024) doi:10.20944/preprints202310.1685.v1.

67. Whittington, C. M., Danastas, K., Grau, G. E., Murphy, C. R. & Thompson, M. B. Expression of VEGF111and other VEGF-A variants in the rat uterus is correlated with stage of pregnancy. *J. Comp. Physiol. B* **187**, 353–360 (2017).

68. Stadtmauer, D. J. & Wagner, G. P. Cooperative inflammation: The recruitment of inflammatory signaling in marsupial and eutherian pregnancy. *J. Reprod. Immunol.* **137**, 102626 (2020).

69. Kumar, S. *et al.* TimeTree 5: An Expanded Resource for Species Divergence Times. *Mol. Biol. Evol.* **39**, msac174 (2022).

70. Dawkins, R. & Krebs, J. R. Arms Races between and within Species. *Proc. R. Soc. Lond. B Biol. Sci.* **205**, 489–511 (1979).

71. Williams, C. *et al.* An Exon Splice Enhancer Primes IGF2:IGF2R Binding Site Structure and Function Evolution. *Science* **338**, 1209–1213 (2012).

72. McCoy, D. E. & Haig, D. Embryo Selection and Mate Choice: Can ‘Honest Signals’ Be Trusted? *Trends Ecol. Evol.* **35**, 308–318 (2020).

73. Zhou, X. *et al.* Circuit Design Features of a Stable Two-Cell System. *Cell* **172**, 744-757.e17 (2018).

74. Gupta, A. & Suzumura, T. Finding All Bounded-Length Simple Cycles in a Directed Graph. Preprint at https://doi.org/10.48550/arXiv.2105.10094 (2021).

75. Ramsey, E. M. *The Placenta: Human and Animal*. (Praeger, New York, NY, US, 1982).

76. Cornelis, G. *et al.* Retroviral envelope gene captures and syncytin exaptation for placentation in marsupials. *Proc. Natl. Acad. Sci.* **112**, E487–E496 (2015).

77. Cornelis, G. *et al.* Retroviral envelope syncytin capture in an ancestrally diverged mammalian clade for placentation in the primitive Afrotherian tenrecs. *Proc. Natl. Acad. Sci.* **111**, E4332–E4341 (2014).

78. Vernochet, C. *et al.* A syncytin-like endogenous retrovirus envelope gene of the guinea pig specifically expressed in the placenta junctional zone and conserved in Caviomorpha. *Placenta* **32**, 885–892 (2011).

79. Lynch, V. J., Leclerc, R. D., May, G. & Wagner, G. P. Transposon-mediated rewiring of gene regulatory networks contributed to the evolution of pregnancy in mammals. *Nat. Genet.* **43**, 1154–1159 (2011).

80. Henthorn, C. R., Airs, P. M., Neumann, E. K. & Zamanian, M. Resolving the origins of secretory products and anthelmintic responses in a human parasitic nematode at single-cell resolution. *eLife* **12**, e83100 (2023).

81. Hu, M., Bai, Y., Zheng, X. & Zheng, Y. Coral–algal endosymbiosis characterized using RNAi and single-cell RNA-seq. *Nat. Microbiol.* **8**, 1240–1251 (2023).

Methods

Animal Husbandry

Pregnant samples were taken at gestation points after the establishment of the definite placenta and, in the case of mice and guinea pigs, before the luteal-placental shift in progesterone secretion.

M. domestica were raised in a breeding colony at Yale University according to established technical protocols[1] and ethical protocols approved by the Yale University Institutional Animal Care and Use Committee (#2020-11313). Male and female animals were housed separately after 3 months of age, at which point female opossums were introduced to the male room for sexual preconditioning, and breeding was attempted after 6 months. During breeding, non-cycling female opossums were introduced to the male room for 1 day, and then subsequently swapped into the used cage of a prospective male partner for 5 days. After this period, both individuals were placed into a breeding cage and video recorded to assess the time of copulation. If multiple copulations were observed, the first was always used to calibrate 0 dpc; samples were taken one day before parturition at 13.5 dpc (n=2).

T. ecaudatus were maintained in a breeding colony at the University of Nevada, Las Vegas according to established Institutional Animal Care protocols. Individuals in the colony descend from a population of 40 wild-caught animals imported from Mauritius in June 2014. Animals were mated and mid-gestation was sampled for scRNA-seq between 28 and 29 days (n=3; staging data in **Suppl. Table 9**) following the first exposure of females to males.

C. porcellus (Charles River) were maintained at the University of Vienna according to Institutional Animal Care protocols. Midgestation samples (n=2) were collected 30.5 days post copulation.

M. musculus (C57BL/6J) were maintained at the University of Vienna and at Yale University according to Institutional Animal Care protocols. Midgestation samples (n=2) were collected 15.5 days post copulation.

Single-Cell RNA Sequencing

Single-cell RNA sequencing was conducted on pregnant opossum uteri at the above developmental stages. Uteri were dissected into phosphate-buffered saline (PBS), separated from the cervix and fallopian tube, and opened longitudinally. In the case of late gestation, embryos and directly attached extraembryonic membranes were removed via severing of the umbilical cords. In mid-gestation, blastocysts were flushed from the uterus with saline delivered through a syringe inserted into the anterior end to verify pregnancy but not sequenced. Tissue samples were kept at 4°C for approximately 30 minutes until they could be dissociated into a single-cell suspension according to a protocol modified from[2].

Tissue was minced with a scalpel into ~1 mm^3 cubes in 2 mL of digestive solution containing 0.2 mg/mL Liberase TL (05401020001, Sigma). Tissue suspensions were heated at 37°C for 15 minutes and then passed 10 times through a 16-gauge needle attached to a 3-mL syringe. This incubation and needle passage process was repeated two more times, with the substitution of an 18-gauge needle. Finally, 2 mL of charcoal-stripped fetal bovine serum (100-199, Gemini) was added and the suspension was immediately passed through a 70-µm cell strainer then a 40-µm cell strainer. The flowthrough was pelleted by centrifugation at 500 g for 5 minutes and cells were resuspended in 1x ACK red blood cell lysis buffer (A1049201, Thermo-Fisher), incubated at room temperature for 5 minutes, centrifuged again and resuspended in PBS containing 0.04% bovine serum albumen (A9647,

Sigma). At this point, cells were examined on a hemocytometer to gauge concentration and check for debris and cell death using trypan blue stain (15250061, ThermoFisher).

Cells were captured using the 10X Chromium platform (3' chemistry, version 3), libraries were generated according to manufacturer protocols (CG000315), and sequenced using an Illumina NovaSeq apparatus.

Laser Microdissection Verification

Microbulk transcriptomes were generated from laser-microdissected cryosections of 13.5 dpc bilaminar omphalopleure of the opossum (n=3) to verify that pro-inflammatory putative fetal cells were indeed placental in origin (**Suppl. Figure 6**). Samples for this procedure were dissected into PBS and subsequently immersed Tissue-Tek OCT compound (Sakura Finetek, 4583) in a block mold and flash frozen by exposure to a bath of isopentane surrounded by dry ice, and stored at -80°C. 14-µm sections were prepared from the resulting blocks on a cryomicrotome (Microm HM 500 OM) and placed onto polyethylene napthalate membrane slides (Leica Microsystems, 11505158) which had been exposed to UV irradiation in a biosafety cabinet (Baker SterilGARD, SG-404) for 30 minutes. Sections were processed on a Leica LMD7000 apparatus and excised tissue dropped directly into lysis buffer for processing using a Qiagen RNeasy Micro Kit (74004). RNA libraries were prepared by the Yale Center for Genomic Analysis using a NEBNext Low Input Library Prep Kit (E6420) and sequenced using an Illumina NovaSeq apparatus. Reads were aligned to the transcriptomes used for scRNA-seq analysis using kallisto (0.45.0)[3].

Histology and Histochemistry

Histological samples were fixed for 24 hours in 10% neutral buffered formalin, followed by dehydration to 70% Ethanol and kept at 4°C (days-weeks) or -20°C (months) before paraffin embedding. Staining with Gill 2 hematoxylin and Y alcoholic eosin was performed according to[4]. Bright-field images for Figure 1 were taken with a Leica Thunder Imager (*Tenrec*), a Nikon Eclipse E600 (*Monodelphis*), and an EVOS scanning microscope (*Cavia* and *Mus*).

Immunohistochemistry was performed using the following antibodies:

Target	**Antibody Species + Clonality**	**Target Region (if known)**	**Manufacturer ID**	**Concentration Used**	**Western Blot Verification**
GPC1	Rabbit polyclonal		ab226855	1:200	
HOXA11	Goat polyclonal	144-193 of NP_005514	sc-48542	1:1000[5]	Kin et al. (2014)
Cytokeratin AE1+AE3	Mouse monoclonal		CF190321	1:200	
KRT7	Rabbit monoclonal		ab181598	1:200	
KRT19	Rabbit monoclonal		ab52625	1:1000	

SMOC1	Rabbit polyclonal		ab200219	1:200	
TFAP2C	Rabbit monoclonal		ab76007	1:250	
Goat IgG	Donkey		sc-2056	1:5000	N/A
Rabbit IgG	Goat		ab150077	1:1000	

For HOXA11 immunohistochemistry, slides were incubated for 1 hour at 65°C, dewaxed with xylene, washed in 100% ethanol, and rehydrated in running tap water. Antigen retrieval was performed for 1 hour in a 95°C vegetable steamer containing 10 uM sodium citrate (pH 6.0). Slides were washed in phosphate-buffered saline and blocked with 0.1% mass/volume bovine serum albumen. Peroxidases were blocked by incubation in 0.03% hydrogen peroxide containing sodium azide (DAKO) in a humidification chamber for 30 minutes. Slides were incubated overnight at 4°C in primary antibody solutions, blocked, treated with horseradish peroxidase-conjugated secondary antibody for 1 hour at room temperature. Finally, slides were washed in blocking solution once more and treated with 3,3'-diaminobenzidine (DAKO K401011-2) for 5 minutes and counterstained with Gill 2 hematoxylin before brightfield imaging.

For fluorescent immunohistochemistry, the procedure had the following modifications. Peroxidase blocking and 3,3'-diaminobenzidine was not used in favor of fluorescent secondary antibodies. Fluorescent images were taken using an EVOS microscope. Fluorescent images were also captured in the red channel and superimposed to leverage the autofluorescent nature of mammalian erythrocytes and highlight the location of vasculature.

In Situ Hybridization

Single-molecule fluorescence *in situ* hybridization was conducted on formalin-fixed paraffin-embedded sections using the RNAscope platform following the manufacturer's protocols (ACD Bio 323100-USM for fluorescent and 322310-USM for chromogenic). Probes were designed against the equivalent transcript sequences used for RNA-seq alignment and deposited into the RNAscope database as standardized probes. Probes used were the following:

Species	**Gene**	**Visualization**	**Target Region (NCBI)**	**Manufacturer ID**
Monodelphis domestica	*FBLN1*	Opal 570	887-1837 of XM_001378451.3	1144361-C3
Monodelphis domestica	*SMOC2*	Opal 520	417-1357 of XM_007484917.2	1144381-C4
Monodelphis domestica	*IL6*	Opal 620	2-1078 of XM_007505389.2	1144611-C2
Monodelphis domestica	*GCM1*	Chromogenic (diaminobenzidine)	409-1519 of XM_007484095.1	1144871-C1

Monodelphis domestica	*HAND1*	Chromogenic (diaminobenzidine)	125-877 of ENST00000231121.HAND1.2	1264181-C1
Monodelphis domestica	*KRT18*	Chromogenic (diaminobenzidine)	11-1305 of XM_001377456.3	1146551-C1
Tenrec ecaudatus	*IL15*	Chromogenic (diaminobenzidine)	392-1059 of de novo transcript	1264191-C1
Tenrec ecaudatus	*KRT18*	Chromogenic (diaminobenzidine)	123-1659 of de novo transcript	1324401-C1
Tenrec ecaudatus	*HAND2*	Chromogenic (diaminobenzidine)	878-2014 of de novo transcript	1304911-C1
Cavia porcellus	*PRL (ENSCPOG00000023538)*	Chromogenic (diaminobenzidine)	2-496 of ENSCPOT00000022559.2	1294841-C1
Bacillus subtilis	*DapB* (negative control)			310043

Fluorescent RNAscope was performed using the MultiPlex platform (ACD Bio 323100) with Opal 520, Opal 570, Opal 620, and Opal 690 fluorophores (Akoya Biosciences). Fluorescent images were captured using a laser scanning confocal microscope (Leica Stellaris 8 Falcon). For Figure 3b, Fluorescent images were also captured at 690 nm and superimposed to leverage the autofluorescent nature of the opossum glands to highlight the location of glandular epithelia. Chromogenic RNAscope was performed using the RNAscope 2.5 HD Brown Assay (ACD Bio 322300) and imaged on an EVOS microscope.

Single-Cell Data Analysis

Reads were aligned to reference genomes using the 10X Genomics CellRanger software (>=v7.0.0). *Monodelphis domestica*, *Cavia porcellus*, and *Mus musculus* were mapped to their respective Ensembl genome annotations (ASM229v1, cavPor3, and GRCm38) from the version 104 release[6]. For *Tenrec ecaudatus* a novel unpublished genome was provided by the laboratory of Michael Hiller and Fauna Bio, annotated using the TOGA pipeline[7].

Quality control included filtering cells with low count (less than 700 unique features) or high mitochondrial gene expression (more than 25%), as well as doublet detection by scrublet v0.2.3[8] and doubletdetection v4.2[9] to remove clusters consisting of majority doublets. Normalization, feature selection, scaling, and linear dimensional reduction were performed using Scanpy ≥ v1.9.1[10], with the exception of the mouse, which was annotated using equivalent functions in Seurat v4[11] and exported as raw counts and then reprocessed in Scanpy, and the human, which was annotated according to ([12]). Biological replicates were integrated with harmony (harmonypy v0.0.9, r-harmony v0.1)[13]. Fetal cells were identified by a combination of placenta-specific marker gene expression, and non-overlap with non-pregnant uterine samples. In the case of the tenrec which was sufficiently outbred, single nucleotide polymorphism-based inference of the genome of origin using souporcell v2.5[14] (**Suppl. Figure 14**). Spliced and unspliced transcript calling was performed using velocyto (v0.17.17)[15] and RNA velocity analysis by scVelo (v0.30)[16] (**Suppl. Figure 7**).

Because the ground-truth database was curated from the human literature and insufficient data exists to curate ligand-receptor pairs for each species, the non-human transcriptomes were converted into "human-equivalent transcriptomes" by mapping of genes to their top human ortholog as detected by BLAST of translated peptide sequence[17]. To maimize coverage, in cases of many:one human orthology, counts of all detected paralogs were added together. This transformed expression matrix was used only for cell communication analysis and cell phylogeny inference. Dimensional reduction, cluster identification, differential expression testing, and marker gene plotting were all conducted on the unadulterated species-relevant gene sets.

Cell Type Phylogeny

A phylogenetic tree of cell type transcriptomes was calculated using cell type-aggregated transcriptomes from all species, with orthology resolved using the human BLAST method described above. Clusters with high annotation uncertainty, extremely low capture rate, or possible artifactual nature ('Md_LE-OAT', 'Te_T-gd', 'Md_PMN-NE', 'Mm_TC-NKT', 'Mm_NEU', 'Te_NEU-CHL1', 'Hs_Granulocytes', 'Mm_fFB-Myoblast', 'Mm_fFB-ribo') were excluded *a priori* from analysis. Gene expression matrices were corrected for "species signal"[18] by linear regression to remove the species of origin covariate from cell transcriptomes with the scanpy.pp.regress_out() function. A euclidean distance matrix between cell type transcriptomes was then calculated and a neighbor-joining tree generated using the TreeMethods python package (v1.0.3; https://github.com/BradBalderson/TreeMethods). An alternative tree was also generated using the same approach with the additional subsetting of genes to only those annotated as transcription factors in ([19]). Cartoons of cell types are modified from BioRender, ([20]), ([21]), and original art.

Homology Inference by SAMap

SAMap (v.1.3.4)[17] was used to calculate gene homology-aware similarity scores between cells of different species. BLAST (v2.14.1)[22] graphs were generated from the ENSEMBL proteomes of respective species, with the exception of *Tenrec ecaudatus* for which the transcriptome was used with tblastx mode. SAMap mapping tables were exported and analyzed using hierarchical clustering (seaborn v0.13.1) as well as network analysis (networkx v3.2.1)[23]. For network analysis, SAMap mapping scores were used as edge weights and cell types as nodes. Communities were detected using the Leiden algorithm (leidenalg v0.10.2)[24]. Stability of the resulting communities was assessed by repeating community detection with a range of 10000 random initial states and constructing a co-occurrence matrix between cell types: cluster stability was defined as the mean of all cooccurrence values between members of the final community.

Gene Expression Program Identification and Cross-Species Comparison

cNMF v1.4.1[25] was used to infer gene expression programs from count matrices of each species. Analysis was performed following a modified protocol from[26]. Optimal numbers of factors (K) were chosen based upon manual examination of stability-error curves over a range of possible K values from 10-50, selecting a value immediately preceding a sudden drop in stability score (**Suppl. Figure 2**).

For cross-species comparison, spectra scores (i.e. gene loadings) from cNMF were used. Non-human genes were mapped to their closest human orthologs, and in cases of many-to-one mapping, the highest loading score was used. Pearson correlation was calculated between programs and hierarchical clustering conducted using the seaborn (v0.13.1) clustermap function.

Cell-Cell Communication Analysis

Putative cell interactions were inferred using a combination of expression thresholding, followed by statistical testing for significantly cell type-enriched interactions. A ground truth ligand-receptor database was built by manually extending CellPhoneDB v5.0.0[27] with additional curation and metadata This list is archived at https://gitlab.com/dnjst/ViennaCPDB/. From these transcriptomes and the ground-truth list, interaction scores for all cell type pairs were generated using the LIANA+ (v1.0.3)[28] and chinpy (https://gitlab.com/dnjst/chinpy) frameworks.

For co-evolutionary integration analysis, all ligand-receptor interactions in the ground truth database were classified into “off” (ligand and receptor off), “allocrine ligand” (ligand on, receptor off), “allocrine receptor” (receptor on, ligand off), and “autocrine” (ligand and receptor on) states, based upon an expression threshold of 20% of cells in a cluster.

For lineage-specific growth factor analysis, growth factor interactions were defined as those where ligands belong to the gene ontology “growth factor” category (GO:0008083). Lineage-specificity of growth factor interactions was estimated by constructing a directed signaling graph for each growth factor ligand-receptor pair, with edge weights equal to the negative natural log of the LIANA+ “magnitude_rank” value for the interaction (a robust rank aggregate p-value of the program’s default statistical tests designed to test signaling magnitude). Weighted in-degrees for each cell type, sum of all incoming edge weights, were calculated, and the Gini coefficient of the resulting weighted in-degree distribution was calculated. Gini coefficients were also calculated on the distribution of HITS authority scores rather than cell type in-degree, and found not to differ substantially.

For disambiguation analysis, a manually-corrected version of CellPhoneDB “classification” metadata was used to group ligands into ligand families. To preserve gene duplication events, in cases of many-to-one homology, all possible homologs to the human ground truth ligand list were included in the target species’ ligand family using Ensembl (mouse, guinea pig, opossum) or BLAST (tenrec) orthology. Expected values of disambiguated ligands were calculated as described in Statistical Analysis.

For discrete ancestral state reconstruction, interactions were scored in a boolean on/off manner based on a nonzero expression threshold of 10% of cells in a cluster for all subunits of both ligand and receptor. Maximum parsimony was calculated using the castor package (v1.8.0)[29]. For continuous ancestral state reconstruction, restricted maximum likelihood was used via the ape package (v5.8)[30] as in[31].

Statistical Analysis

For cell-cell communication inference, single-cell transcriptomes from multiple biological replicates (sample sizes reported above) were pooled before inference of cell communication was performed, following common practice across communication inference methods[32]. Instead of biological replicate-based testing, other statistical tests, such as CellPhoneDB[33] and CellChat[34] permutation tests, are standard; output from these tests (calculated as described above using LIANA+) are available for ligand-receptor interactions of all species as **Supplementary Data**. Likewise, the small sample size of scRNA-seq studies complicates statistical testing of differential cell type abundance[35], so the relative abundance measures in **Figure 1c** are presented as pooled values.

Disambiguation of ligands was compared to a null model in which the probability of randomly redistribution of ligands to cell types leading to exclusively maternal or exclusively fetal expression is assessed. First, all secreted peptide and small molecule-mediated ligand-receptor interactions were classified into “fetal-only”, “maternal-only”, or “both” expression groups based on the threshold value of 20% or more of the cells sequenced expressing the ligand in. Ligands were grouped into ligand families using an additionally curated version of the CellPhoneDB “classification” metadata

(CellPhoneDB v5.1.0). For each ligand family, the per-cell type probability of a given ligand being expressed was calculated according to the equation:

$$P_{on} = \frac{L_{expressed}}{S_{pathway} \times (N_{fetal} + N_{maternal})}$$

where $L_{expressed}$ is the observed number of "on" calls within the ligand family across fetal and maternal cell types, N_{fetal} is the number of fetal cell types, $N_{maternal}$ the number of maternal cell types, and $S_{pathway}$ the number of ligands in the family.

The null probabilities of fetal-only and maternal-only expression for a ligand, respectively, were given by:

$$P_{fetalonly} = \left(1 - (1 - P_{on})^{N_{fetal}}\right) \cdot (1 - P_{on})^{N_{maternal}}$$

$$P_{maternalonly} = \left(1 - (1 - P_{on})^{N_{maternal}}\right) \cdot (1 - P_{on})^{N_{fetal}}$$

The expected fetal-only and maternal-only ligands in each family were obtained by multiplying $P_{fetalonly}$ and $P_{maternalonly}$ by the number of ligands in the family.

Finally, a one-way chi-squared goodness of fit test (scipy.stats.chisquare v1.12.0) for identity of observed and expected counts of the 3 scoring categories (coexpressed, fetal-only, and maternal-only) was used to obtain chi-squared and p-values, with individual observations corresponding to ligands within a family. The Benjamini-Hochberg correction was used (statsmodels.multitest.multipletests v0.14.1) with an alpha of 0.05 to obtain false discovery rate q-values. For plotting, ligand families were considered significant if $p \leq 0.05$ and $q \leq 0.05$. Bonferroni-corrected p-values, obtained by multiplying *p* by the number of ligands in a family, is also reported in **Suppl. Table 5**.

Code Availability

Code used to produce figures and major analyses will be made available at https://github.com/dnjst/fmi2024.

Methods References

1. Keyte, A. L. & Smith, K. K. Basic Maintenance and Breeding of the Opossum Monodelphis domestica. *Cold Spring Harb. Protoc.* **2008**, pdb.prot5073 (2008).
2. Suryawanshi, H. *et al.* A single-cell survey of the human first-trimester placenta and decidua. *Sci. Adv.* **4**, eaau4788 (2018).
3. Bray, N. L., Pimentel, H., Melsted, P. & Pachter, L. Near-optimal probabilistic RNA-seq quantification. *Nat. Biotechnol.* **34**, 525–527 (2016).
4. Kiernan, J. *Histological and Histochemical Methods*. (Scion Publishing Ltd, 2015).
5. Kin, K., Maziarz, J. & Wagner, G. P. Immunohistological Study of the Endometrial Stromal Fibroblasts in the Opossum, Monodelphis domestica: Evidence for Homology with Eutherian

Stromal Fibroblasts1. *Biol. Reprod.* **90**, (2014).

6. Howe, K. L. *et al.* Ensembl 2021. *Nucleic Acids Res.* **49**, D884–D891 (2021).
7. Kirilenko, B. M. *et al.* Integrating gene annotation with orthology inference at scale. *Science* **380**, eabn3107 (2023).
8. Wolock, S. L., Lopez, R. & Klein, A. M. Scrublet: Computational Identification of Cell Doublets in Single-Cell Transcriptomic Data. *Cell Syst.* **8**, 281-291.e9 (2019).
9. Gayoso, A. & Shor, J. JonathanShor/DoubletDetection: doubletdetection v4.2. Zenodo https://doi.org/10.5281/zenodo.6349517 (2022).
10. Wolf, F. A., Angerer, P. & Theis, F. J. SCANPY: large-scale single-cell gene expression data analysis. *Genome Biol.* **19**, 15 (2018).
11. Hao, Y. *et al.* Integrated analysis of multimodal single-cell data. *Cell* **184**, 3573-3587.e29 (2021).
12. Arutyunyan, A. *et al.* Spatial multiomics map of trophoblast development in early pregnancy. *Nature* **616**, 143–151 (2023).
13. Korsunsky, I. *et al.* Fast, sensitive and accurate integration of single-cell data with Harmony. *Nat. Methods* **16**, 1289–1296 (2019).
14. Heaton, H. *et al.* Souporcell: robust clustering of single-cell RNA-seq data by genotype without reference genotypes. *Nat. Methods* **17**, 615–620 (2020).
15. La Manno, G. *et al.* RNA velocity of single cells. *Nature* **560**, 494–498 (2018).
16. Bergen, V., Lange, M., Peidli, S., Wolf, F. A. & Theis, F. J. Generalizing RNA velocity to transient cell states through dynamical modeling. *Nat. Biotechnol.* **38**, 1408–1414 (2020).
17. Tarashansky, A. J. *et al.* Mapping single-cell atlases throughout Metazoa unravels cell type evolution. *eLife* **10**, e66747 (2021).
18. Musser, J. M. & Wagner, G. P. Character trees from transcriptome data: Origin and individuation of morphological characters and the so-called “species signal”. *J. Exp. Zoolog. B Mol.*

Dev. Evol. **324**, 588–604 (2015).

19. Lambert, S. A. *et al.* The Human Transcription Factors. *Cell* **172**, 650–665 (2018).

20. Erkenbrack, E. M. *et al.* The mammalian decidual cell evolved from a cellular stress response. *PLOS Biol.* **16**, e2005594 (2018).

21. DiFrisco, J., Love, A. C. & Wagner, G. P. Character identity mechanisms: a conceptual model for comparative-mechanistic biology. *Biol. Philos.* **35**, 44 (2020).

22. Camacho, C. *et al.* BLAST+: architecture and applications. *BMC Bioinformatics* **10**, 421 (2009).

23. Hagberg, A. A., Schult, D. A. & Swart, P. J. Exploring Network Structure, Dynamics, and Function using NetworkX. in *Proceedings of the 7th Python in Science Conference* (eds. Varoquaux, G., Vaught, T. & Millman, J.) 11–15 (Pasadena, CA USA, 2008).

24. Traag, V. A., Waltman, L. & van Eck, N. J. From Louvain to Leiden: guaranteeing well-connected communities. *Sci. Rep.* **9**, 5233 (2019).

25. Kotliar, D. *et al.* Identifying gene expression programs of cell-type identity and cellular activity with single-cell RNA-Seq. *eLife* **8**, e43803 (2019).

26. Brückner, A. *et al.* Evolutionary assembly of cooperating cell types in an animal chemical defense system. *Cell* **184**, 6138-6156.e28 (2021).

27. Garcia-Alonso, L. *et al. Mapping the Temporal and Spatial Dynamics of the Human Endometrium in Vivo and in Vitro*. 2021.01.02.425073 https://www.biorxiv.org/content/10.1101/2021.01.02.425073v1 (2021) doi:10.1101/2021.01.02.425073.

28. Dimitrov, D. *et al.* LIANA+: an all-in-one cell-cell communication framework. 2023.08.19.553863 Preprint at https://doi.org/10.1101/2023.08.19.553863 (2023).

29. Louca, S. & Doebeli, M. Efficient comparative phylogenetics on large trees. *Bioinformatics* **34**, 1053–1055 (2018).

30. Paradis, E. & Schliep, K. ape 5.0: an environment for modern phylogenetics and evolutionary analyses in R. *Bioinformatics* **35**, 526–528 (2019).

31. Ma, X. *et al.* Evolution of higher mesenchymal CD44 expression in the human lineage: A gene linked to cancer malignancy. *Evol. Med. Public Health* **10**, 447–462 (2022).

32. Armingol, E., Officer, A., Harismendy, O. & Lewis, N. E. Deciphering cell–cell interactions and communication from gene expression. *Nat. Rev. Genet.* **22**, 71–88 (2021).

33. Efremova, M., Vento-Tormo, M., Teichmann, S. A. & Vento-Tormo, R. CellPhoneDB: inferring cell–cell communication from combined expression of multi-subunit ligand–receptor complexes. *Nat. Protoc.* **15**, 1484–1506 (2020).

34. Jin, S. *et al.* Inference and analysis of cell-cell communication using CellChat. *Nat. Commun.* **12**, 1088 (2021).

35. Büttner, M., Ostner, J., Müller, C. L., Theis, F. J. & Schubert, B. scCODA is a Bayesian model for compositional single-cell data analysis. *Nat. Commun.* **12**, 6876 (2021).

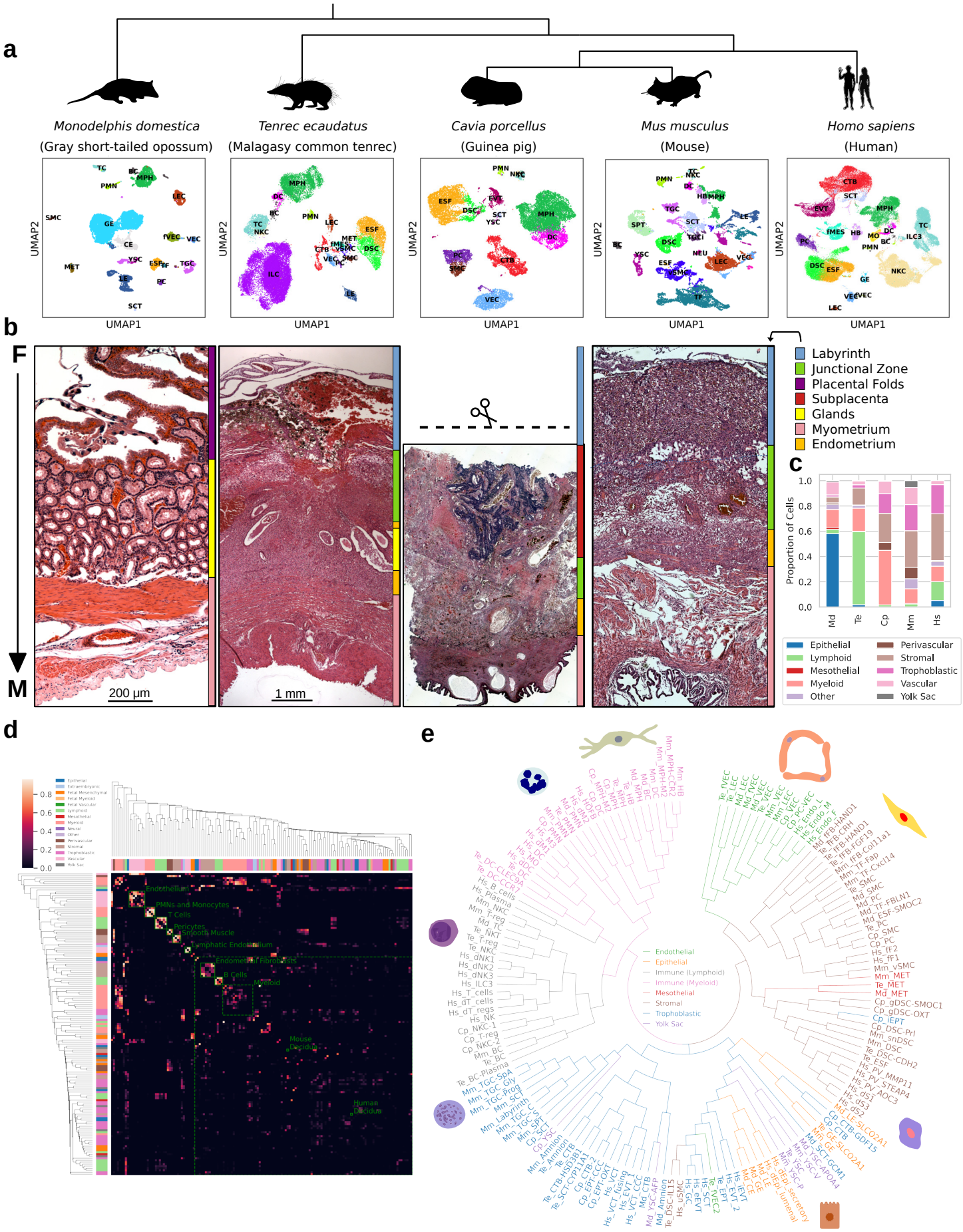
a
Monodelphis domestica
(Gray short-tailed opossum)
Tenrec ecaudatus
(Malagasy common tenrec)
Cavia porcellus
(Guinea pig)
Mus musculus
(Mouse)
Homo sapiens
(Human)
UMAP1
UMAP2
b
F
M
200 µm
1 mm
Labyrinth
Junctional Zone
Placental Folds
Subplacenta
Glands
Myometrium
Endometrium
c
Proportion of Cells
Md
Te
Cp
Mm
Hs
Epithelial
Lymphoid
Mesothelial
Myeloid
Other
Perivascular
Stromal
Trophoblastic
Vascular
Yolk Sac
d
Endothelium
PMNs and Monocytes
T Cells
Pericytes
Smooth Muscle
Lymphatic Endothelium
Endometrial Fibroblasts
B Cells
Myeloid
Mouse Decidua
Human Decidua
e
Endothelial
Epithelial
Immune (Lymphoid)
Immune (Myeloid)
Mesothelial
Stromal
Trophoblastic
Yolk Sac

Figure 1. Single-cell transcriptomic atlases of five mammalian species spanning the diversification of viviparity – from left to right: *Monodelphis domestica*, *Tenrec ecaudatus, Cavia porcellus, Mus musculus, Homo sapiens*. **a.** UMAP embeddings of single-cell transcriptomes from the species listed. **b.** Histology of the fetal-maternal interface of the species in (a). Color bars reflect tissue layers from fetal (F) to maternal (M). **c.** Proportional abundances of cell types belonging to major cell type families in each sample. **d.** Clustered heatmap of pairwise cell type mapping scores (SAMap), with coherent 1:1 orthogroups annotated in green. Row and column colors correspond to cell type families. **e.** A neighbor-joining phylogenetic tree showing hierarchical relationships of cell types recovered, colored by cell type family. For a full list of cell type descriptions, see Supplementary Material. CTB: cytotrophoblast; DC: dendritic cell; DSC/dS1/dS2/dS3: decidual stromal cell; gDSC: giant decidual stromal cell; EPT: extraplacental trophoblast; iEPT: invasive extraplcental trophoblast; EVT: extravillous trophoblast; eEVT: endovascular extravillous trophoblast; iEVT: interstitial extravillous trophoblast; fFB/fMES: fetal mesenchymal cell; GE: glandular epithelial cell; HOFB/HB: Hofbauer cell; ILC: innate lymphoid cell; LE: luminal epithelial cell; LEC: lymphatic endothelial cell; MET: mesothelial cell; MPH: macrophage; NEU: neural cell; NK/NKC: natural killer cells; PC/PV: pericyte; PMN: polymorphonuclear cell; SCT: syncytiotrophoblast; SMC/uSMC: smooth muscle cell; SPT: spongiotrophoblast; TC: T cell; T-reg: regulatory T cell; TF: tissue fibroblast; acTF: activated tissue fibroblast; TGC: trophoblast giant cell; TGC-SpA: spiral artery remodeling trophoblast giant cell; TGC-Prog: progenitor trophoblast giant cell; TGC_Gly: glycogen trophoblast giant cell; TGC_S: sinusoidal trophoblast giant cell; TGC_C: canal trophoblast giant cell; VEC: vascular endothelial cell; fVEC: fetal vascular endothelial cell; YSC: yolk sac cell; YSC-P: parietal yolk sac cell; YSC-V: visceral yolk sac cell.

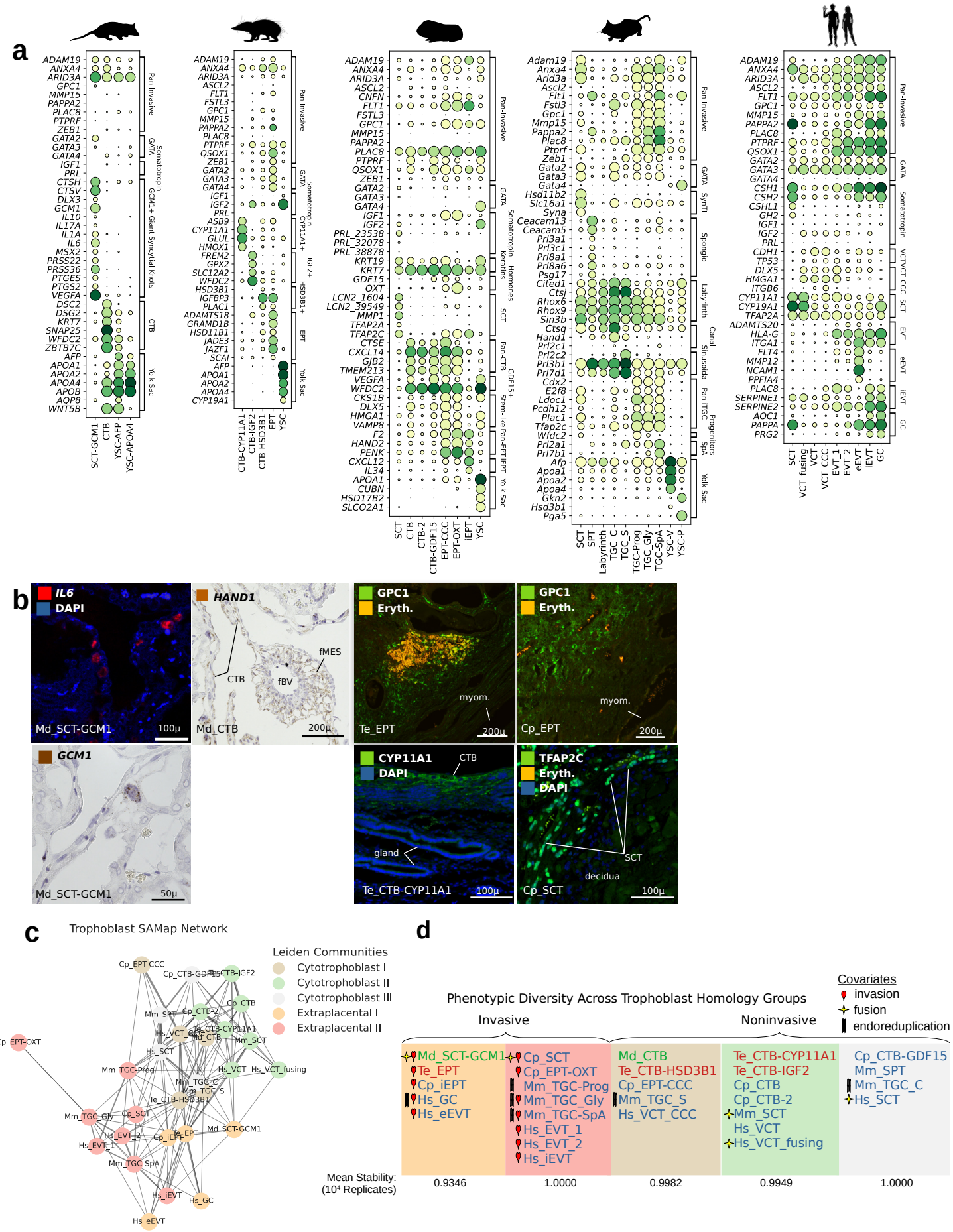

Figure 2. a. Expression of trophoblast marker genes; cell types are clustered by transcription-factor-derived cell type phylogeny. SCT: syncytiotrophoblast; CTB: cytotrophoblast; EPT: extraplacental trophoblast; YSC: yolk sac cell; (T)GC: trophoblast giant cell **b.** Histological localization of select cell type markers from (a). myom.: myometrium; Eryth.: erythrocytes **c.** Network of SAMap linkages between trophoblast cells, with edge thicknesses are proportional to mapping scores. Nodes are colored by inferred Leiden community. **d.** Schematic depiction of phenotypic diversity across trophoblast communities: putative invasiveness groups by community, whereas fusion and endoreduplication are widespread. Md: *Monodelphis domestica*; Te: *Tenrec ecaudatus*; Cp: *Cavia porcellus*; Mm: *Mus musculus*; Hs: *Homo sapiens.* Cell type text colors reflect Marsupialia/Afrotheria/Euarchontoglires distinctions.

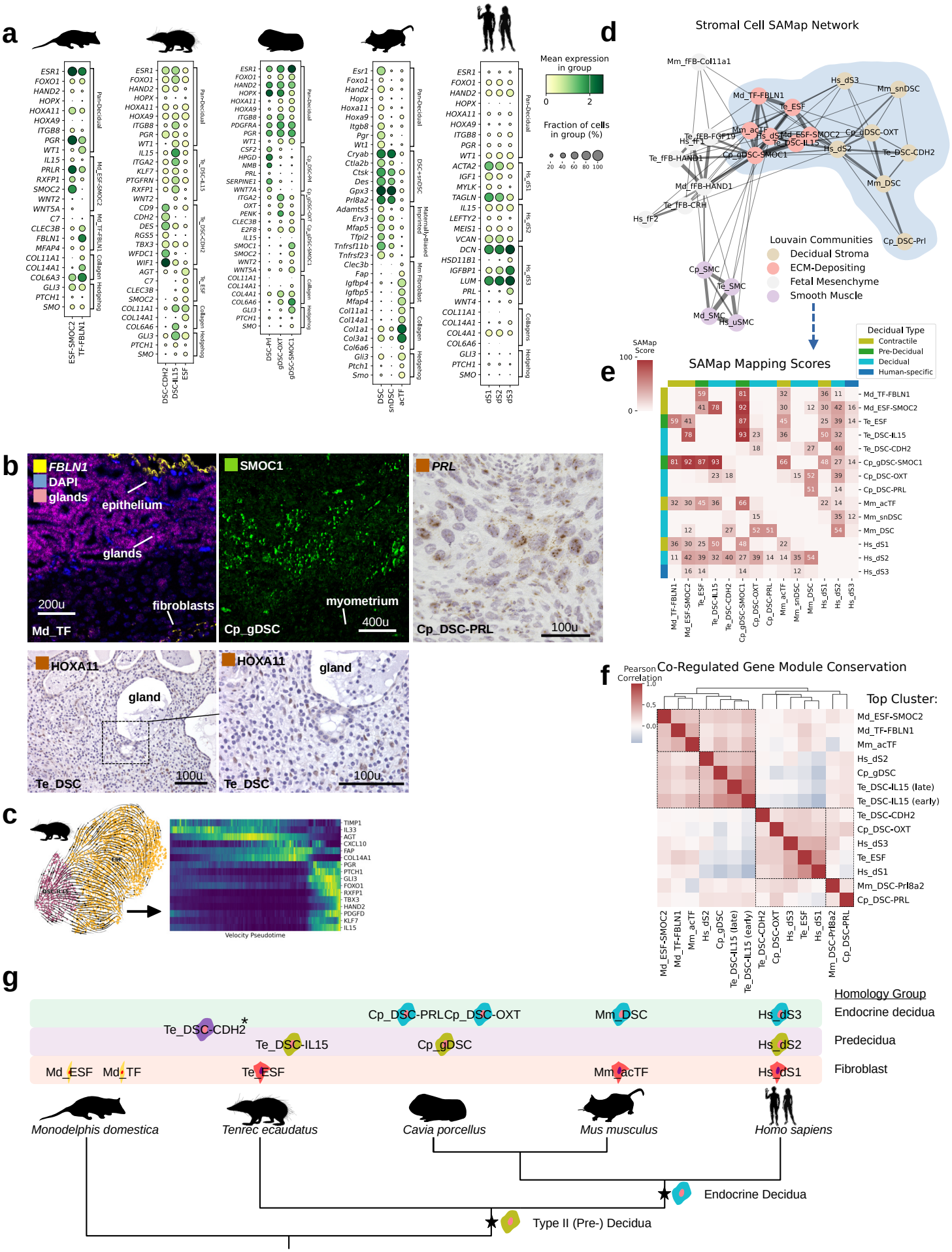

Figure 3. a. Marker gene expression of endometrial stromal and decidual cell types. **b.** *In situ* (italics) and immunohistochemical (upright) localization of select markers genes from (a). **c.** Force atlas embedding of tenrec endometrial stromal cells with RNA velocity vectors overlaid on top. Expression of select top velocity genes in the ESF→DSC transition ordered by velocity-informed pseudotime. **d.** Network of SAMap mapping scores between stromal cell types, with edge weight proportional to mapping scores, colored by louvain cluster. **e.** Heatmap of putative decidual SAMap scores from (d) **f.** Correlation of NMF gene expression programs expressed in decidual stromal cells. **g.** Tree showing inferred evolutionary relationships of decidual subtypes. * denotes uncertain placement of Te_DSC-CDH2.

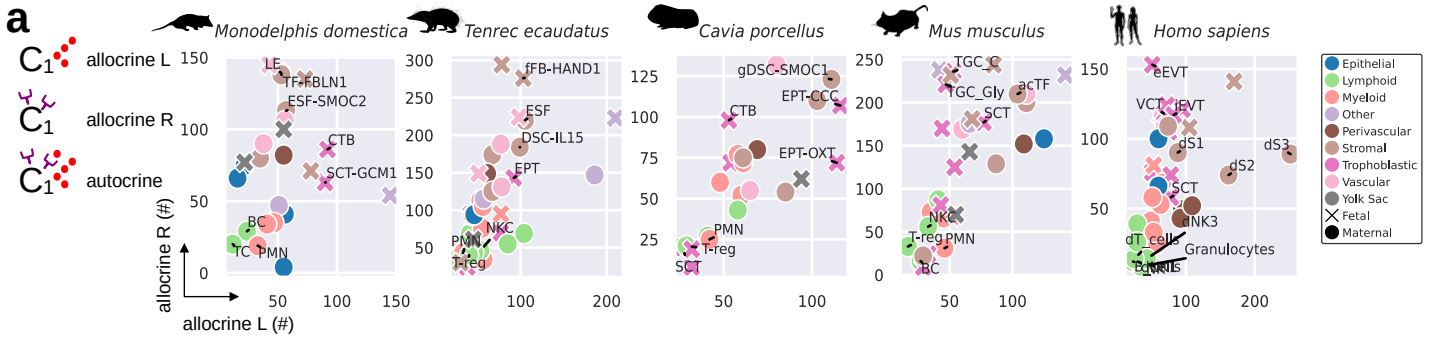
a
Monodelphis domestica
Tenrec ecaudatus
Cavia porcellus
Mus musculus
Homo sapiens
allocrine L
allocrine R
autocrine
allocrine R (#)
allocrine L (#)
Epithelial
Lymphoid
Myeloid
Other
Perivascular
Stromal
Trophoblastic
Vascular
Yolk Sac
Fetal
Maternal

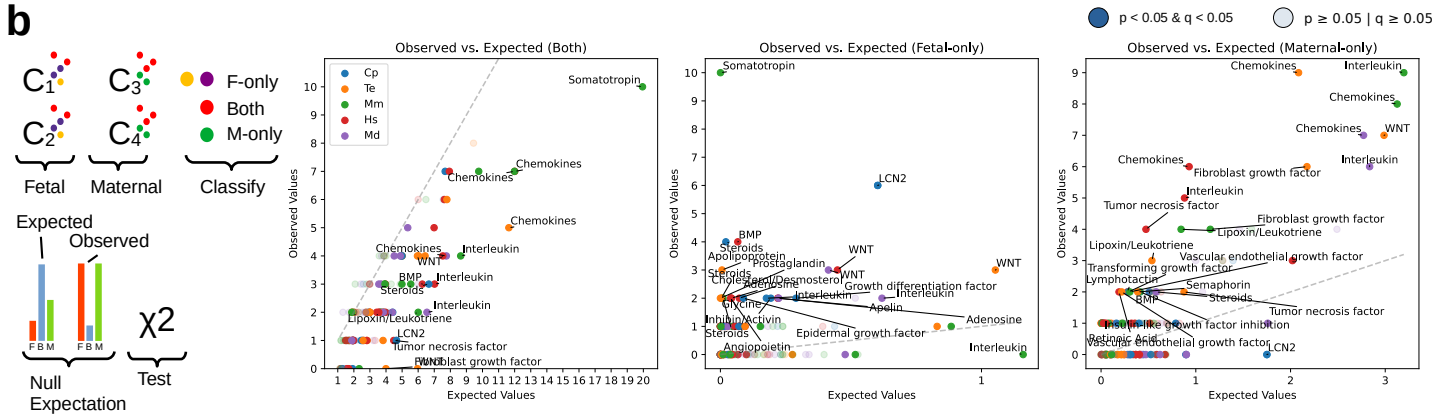
b
p < 0.05 & q < 0.05
p ≥ 0.05 | q ≥ 0.05
F-only
Both
M-only
Fetal
Maternal
Classify
Expected
Observed
Null Expectation
Test
Observed vs. Expected (Both)
Observed vs. Expected (Fetal-only)
Observed vs. Expected (Maternal-only)
Observed Values
Expected Values

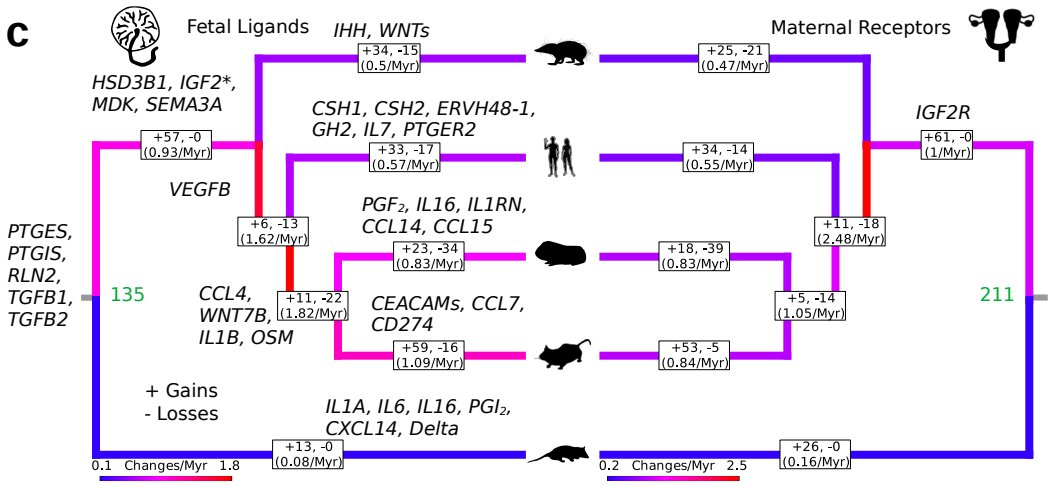
c
Fetal Ligands
Maternal Receptors
IHH, WNTs
HSD3B1, IGF2*, MDK, SEMA3A
CSH1, CSH2, ERVH48-1, GH2, IL7, PTGER2
IGF2R
VEGFB
PGF2, IL16, IL1RN, CCL14, CCL15
PTGES, PTGIS, RLN2, TGFB1, TGFB2
135
211
CCL4, WNT7B, IL1B, OSM
CEACAMs, CCL7, CD274
+ Gains
- Losses
IL1A, IL6, IL16, PGI2, CXCL14, Delta
0.1 Changes/Myr 1.8
0.2 Changes/Myr 2.5

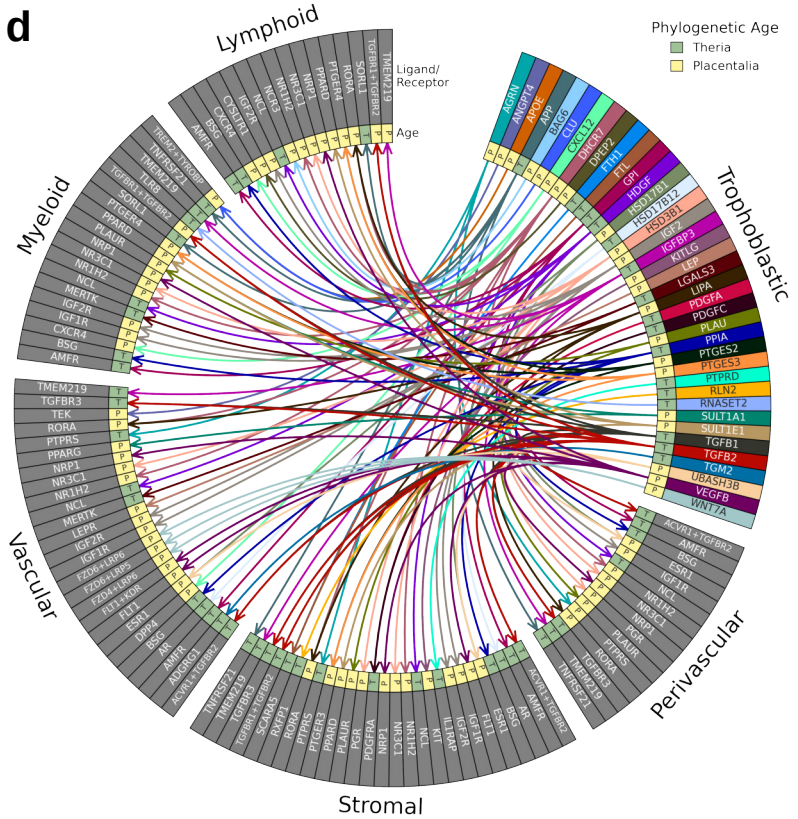
d
Lymphoid
Myeloid
Trophoblastic
Vascular
Perivascular
Stromal
Ligand/ Receptor
Age
Phylogenetic Age
Theria
Placentalia

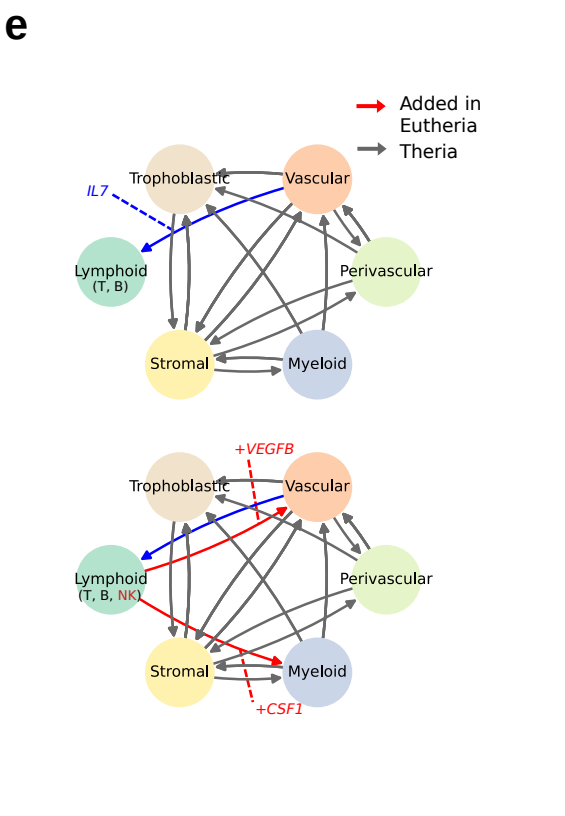
e
Added in Eutheria
Theria
Trophoblastic
Vascular
Lymphoid (T, B)
Perivascular
Stromal
Myeloid
IL7
+VEGFB
Lymphoid (T, B, NK)
+CSF1

Figure 4. Evolutionary dynamics of cell-cell communication. **a.** Expressed allocrine ligands (receptor not produced) and allocrine receptors (ligand not produced) by cell type by species. **b.** Test of disambiguation, showing observed vs. expected numbers of coexpressed, fetal-only, and maternal-only ligands, by ligand family. **c.** Co-evolution of secreted signals by placental cells (left tree) and maternal receptor expression (right tree), as inferred from maximum-parsimony ancestral state reconstruction. Branches are colored by rate (Δ/Myr) using divergence dates from (Kumar et al., 2022 *Mol. Biol. Evol.*). **d.** Reconstructed trophoblast → maternal signaling interactions of Ur-Placentalia, colored by phylogenetic age of the interaction: eutherian novelty (P), ancestral therian (T). **e.** Signaling networks of cell type lineage-specific growth factors between cell classes in the opossum compared to eutherians (identical graphs). Arrows are drawn if ≥ 1 growth factor interaction exists between the two nodes. Arrows belonging to elementary cycles in the graph (i.e. reciprocal signaling) are plotted in gray. Arrows excluded from elementary cycles (i.e., unidirectional signaling) are plotted in blue, and novel eutherian edges in red.

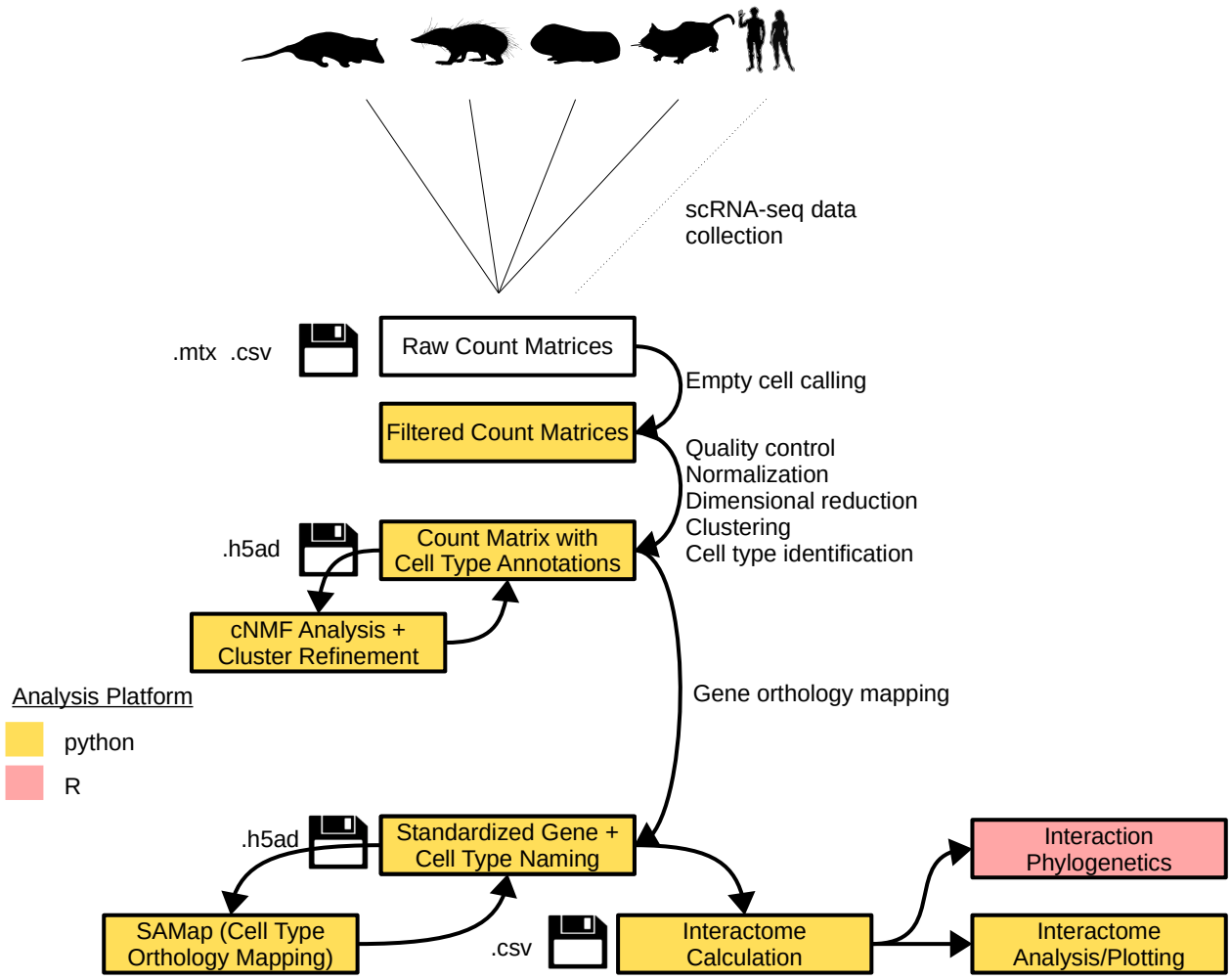

Figure S1. Flow chart of analytical design.

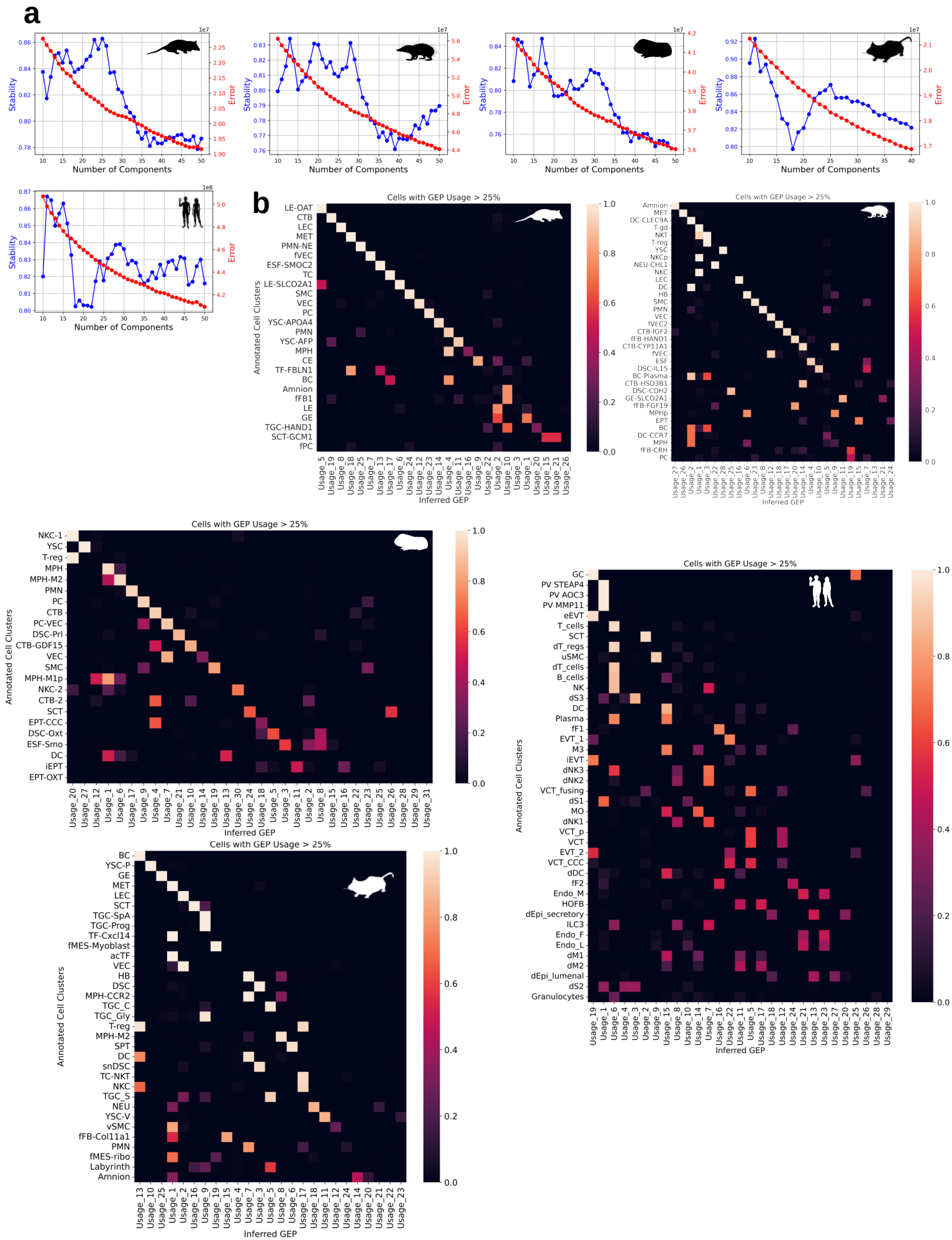

Figure S2. NMF analysis. **a.** Optimal numbers of "gene expression programs" were determined by identifying local stability values preceding a sudden drop. *Monodelphis domestica*: K=26; *Tenrec ecaudatus*: K=28; *Cavia porcellus*: K=31; *Mus musculus*: K=25. *Homo sapiens:* K=29. **b.** Confusion matrices of mean cNMF gene expression program activity scores by cell clusters.

a

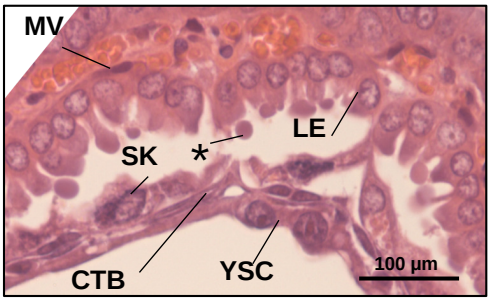
MV
LE
SK
*
CTB
YSC
100 µm

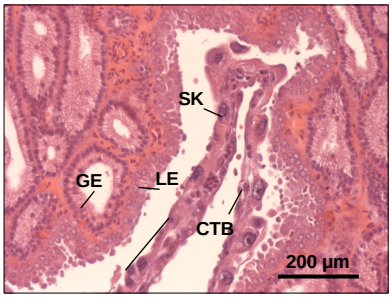
SK
GE
LE
CTB
200 µm

b

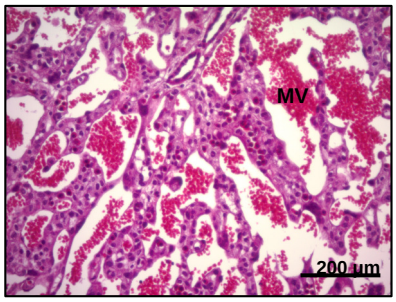
MV
200 µm

c

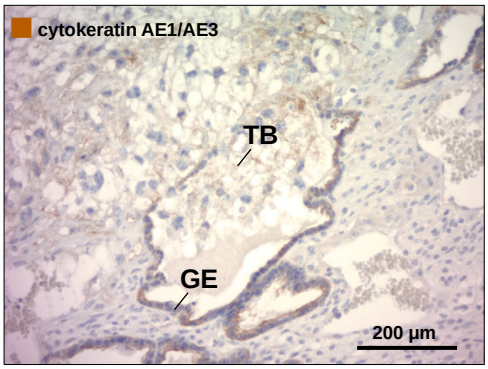
cytokeratin AE1/AE3
TB
GE
200 µm

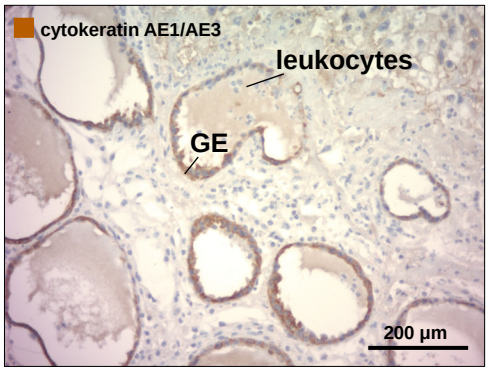
cytokeratin AE1/AE3
leukocytes
GE
200 µm

d

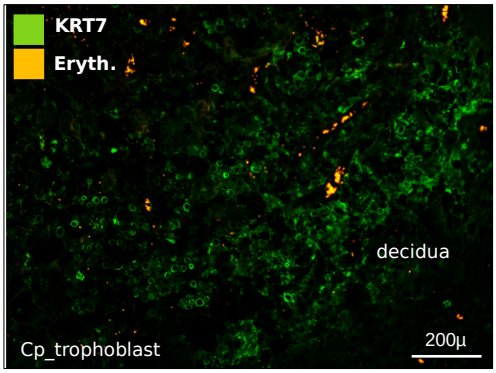
KRT7
Eryth.
decidua
Cp_trophoblast
200µ

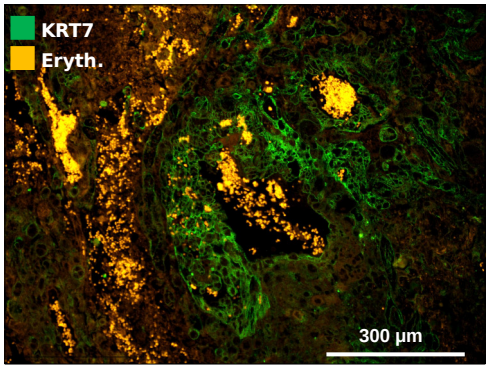
KRT7
Eryth.
300 µm

e

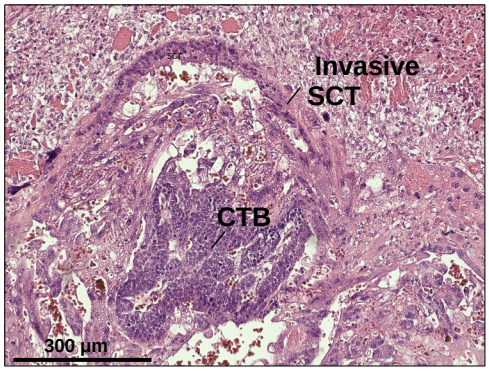
Invasive
SCT
CTB
300 µm

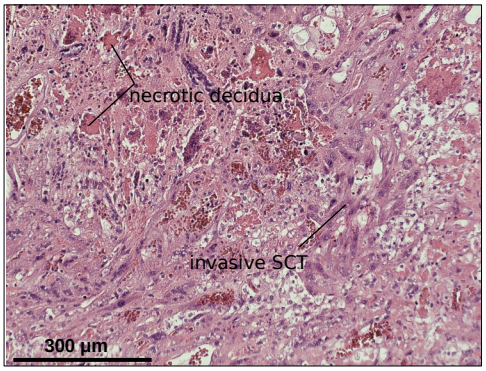
necrotic decidua
invasive SCT
300 µm

f

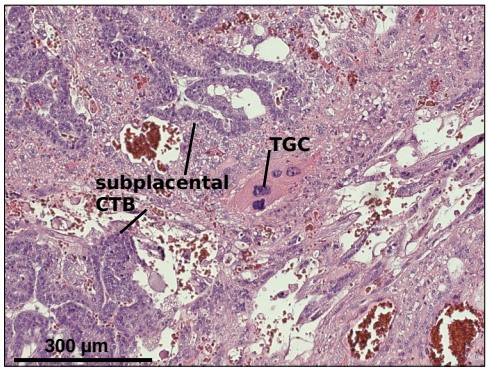
TGC
subplacental
CTB
300 µm

Figure S3. Additional histological identification of cell types. **a.** The opossum fetal-maternal interface. **b.** Placental labyrinth of the tenrec; hematoxylin and eosin stain. **c.** The tenrec invasion front, where trophoblast invades into mucus-filled pores, eroding the lumen positive for cytokeratin (CK AE1/AE3). **d.** KRT7^{+} trophoblast in the guinea pig surrounding decidual stroma (left) and maternal arteries (right). **e.** Invasive SCT in the guinea pig surrounds patches of necrotic stroma. **f.** smFISH for *prolactin* (ENSCPOG000023538) stains a coarse mesh of syncytial cells. Abbreviations: Eryth.: erythrocytes; MV: maternal vasculature; SK: syncytial knot; LE: luminal epithelium; SCT: syncytiotrophoblast; YSC: yolk sac endoderm. GE: glandular epithelium; TB: trophoblast; CTB: cytotrophoblast; *: apocrine secretory body.

a

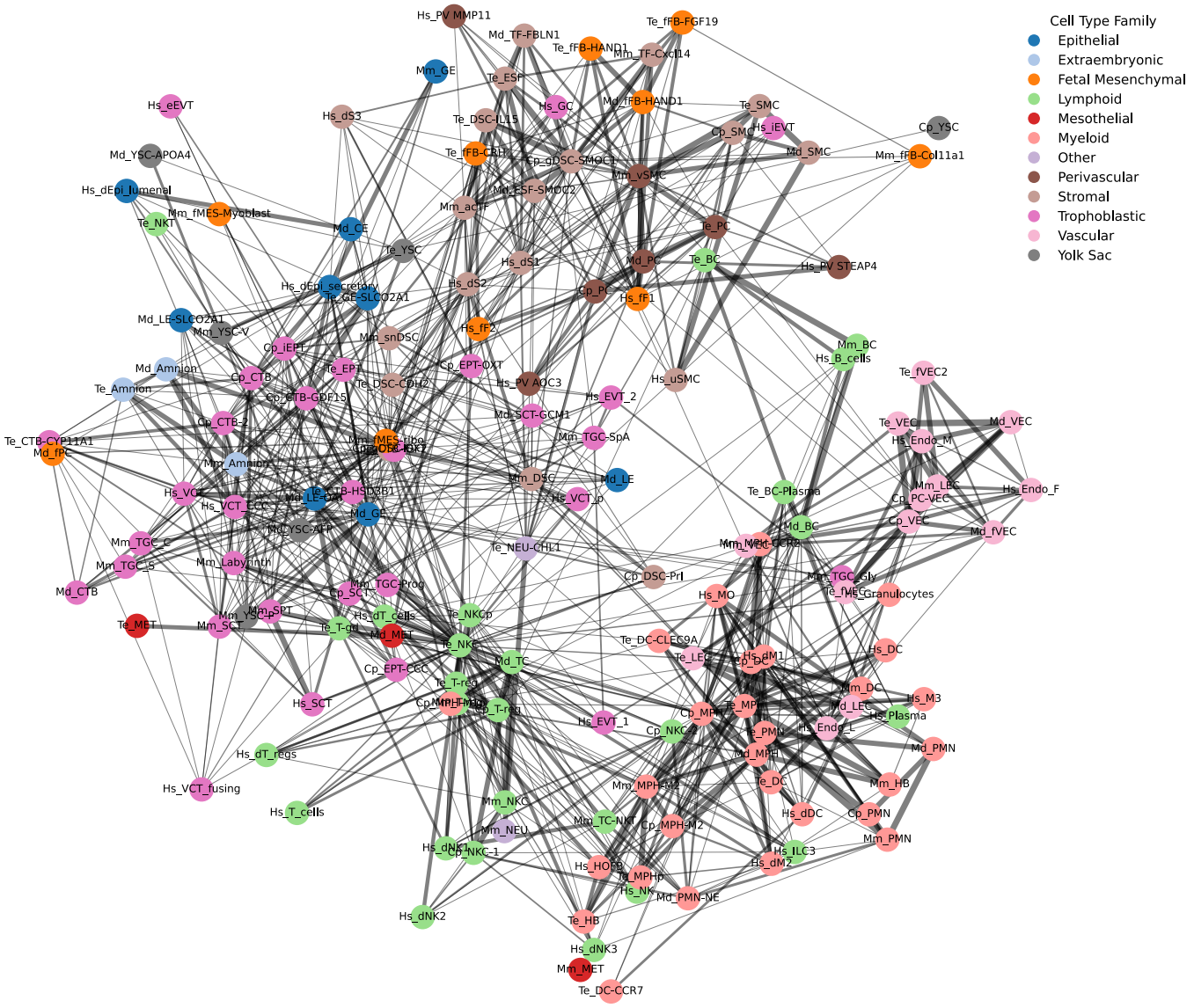
Cell Type Family
Epithelial
Extraembryonic
Fetal Mesenchymal
Lymphoid
Mesothelial
Myeloid
Other
Perivascular
Stromal
Trophoblastic
Vascular
Yolk Sac
Hs_PV MMP11
Md_TF-FBLN1
Te_fFB-FGF19
Te_fFB-HAND1
Mm_TF-Cxcl14
Mm_GE
Te_ESF
Hs_eEVT
Hs_dS3
Hs_GC
Md_fFB-HAND1
Te_SMC
Te_DSC-IL15
Cp_SMC
Hs_iEVT
Cp_YSC
Md_YSC-APOA4
Te_fFB-CRH
Cp_gDSC-SMOC1
Md_SMC
Mm_fFB-Col11a1
Hs_dEpi_lumenal
Mm_vSMC
Md_ESF-SMOC2
Mm_fMES-Myoblast
Mm_acTF
Te_NKT
Md_CE
Te_PC
Te_YSC
Hs_dS1
Md_PC
Te_BC
Hs_PV STEAP4
Hs_dEpi_secretory
Hs_dS2
Te_GE-SLCO2A1
Cp_PC
Hs_fF1
Md_LE-SLCO2A1
Mm_YSC-V
Hs_fF2
Mm_snDSC
Mm_BC
Cp_iEPT
Hs_B_cells
Md_Amnion
Te_EPT
Cp_EPT-OXT
Te_fVEC2
Cp_CTB
Te_DSC-CDH2
Hs_PV AOC3
Hs_uSMC
Te_Amnion
Cp_CTB-GDF15
Hs_EVT_2
Cp_CTB-2
Md_SCT-GCM1
Te_VEC
Md_VEC
Te_CTB-CYP11A1
Mm_TGC-SpA
Hs_Endo_M
Md_fPC
Mm_Amnion
Mm_DSC
Md_LE
Mm_LEC
Hs_Endo_F
Hs_VCT
Te_BC-Plasma
Cp_PC-VEC
Hs_VCT_ECC
Hs_VCT_p
Md_GE
Md_BC
Cp_VEC
Md_YSC-AFP
Md_fVEC
Mm_TGC_C
Te_NEU-CHL1
Mm_TGC_S
Mm_Labyrinth
Cp_DSC-Prl
Mm_TGC_Gly
Md_CTB
Mm_TGC-Prog
Cp_SCT
Hs_MO
Te_MET
Mm_SCT
Hs_dT_cells
Te_NKCp
Te_T-gd
Md_MET
Te_NKC
Te_DC-CLEC9A
Hs_DC
Cp_EPT-CCC
Md_TC
Te_LEC
Hs_dM1
Te_T-reg
Mm_DC
Hs_SCT
Cp_T-reg
Hs_M3
Hs_EVT_1
Cp_MPH
Te_MPH
Md_LEC
Hs_Plasma
Cp_NKC-2
Te_PMN
Hs_Endo_L
Hs_dT_regs
Md_MPH
Md_PMN
Hs_VCT_fusing
Mm_MPH-M2
Te_DC
Mm_HB
Hs_T_cells
Mm_NKC
Hs_dDC
Cp_PMN
Mm_TC-NKT
Cp_MPH-M2
Mm_NEU
Mm_PMN
Hs_dNK1
Cp_NKC-1
Hs_ILC3
Hs_HOFB
Hs_dM2
Te_MPHp
Hs_NK
Md_PMN-NE
Hs_dNK2
Te_HB
Hs_dNK3
Mm_MET
Te_DC-CCR7

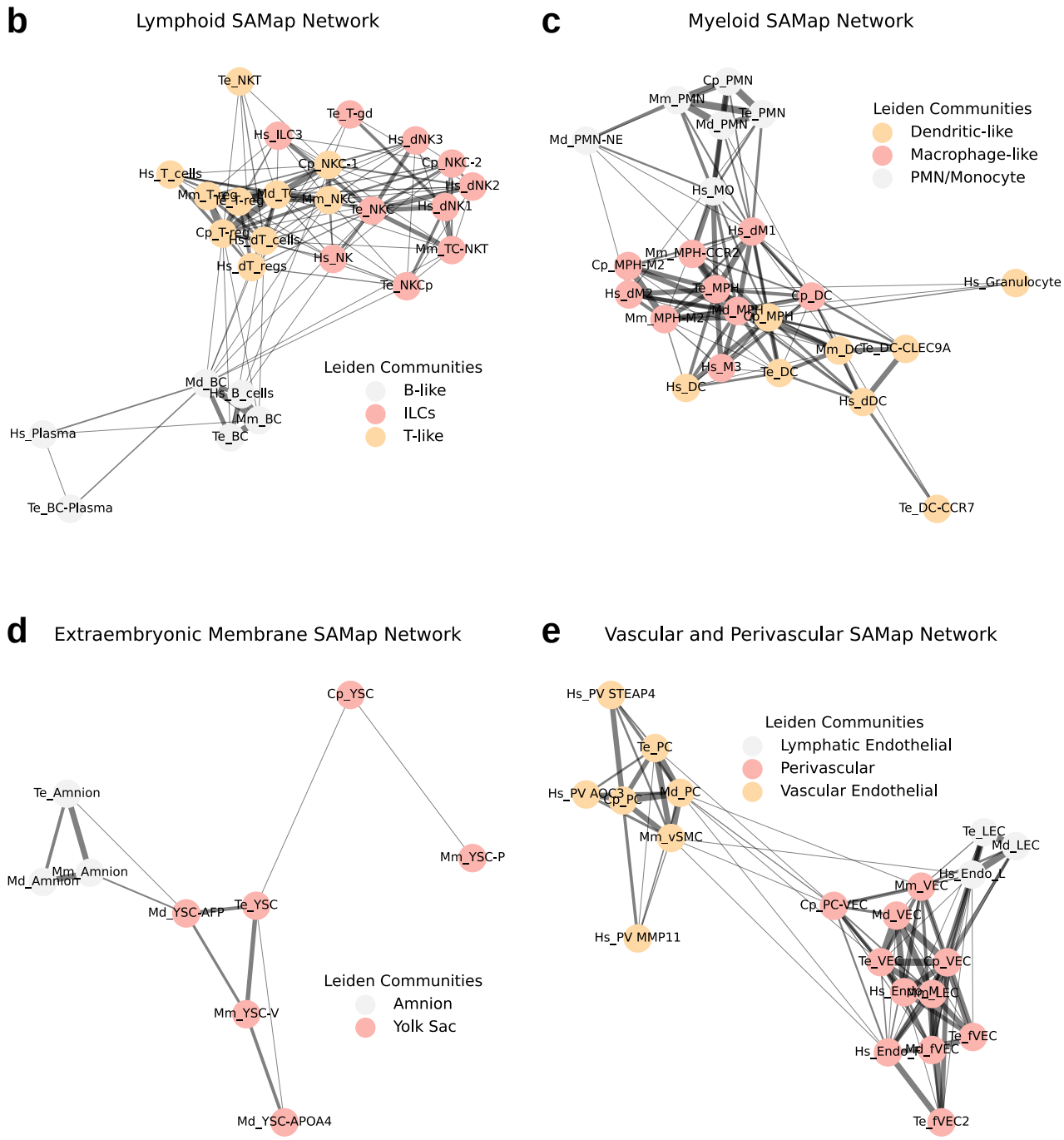

Figure S4 Cell type cross-species mapping scores (SAMap). **a.** Full network constructed from SAMap cross-species cell type mapping scores (0-1), with edge weights equal to score magnitude. **b-e.** Subnetworks of the full network from specific cell type families, colored by leiden community.

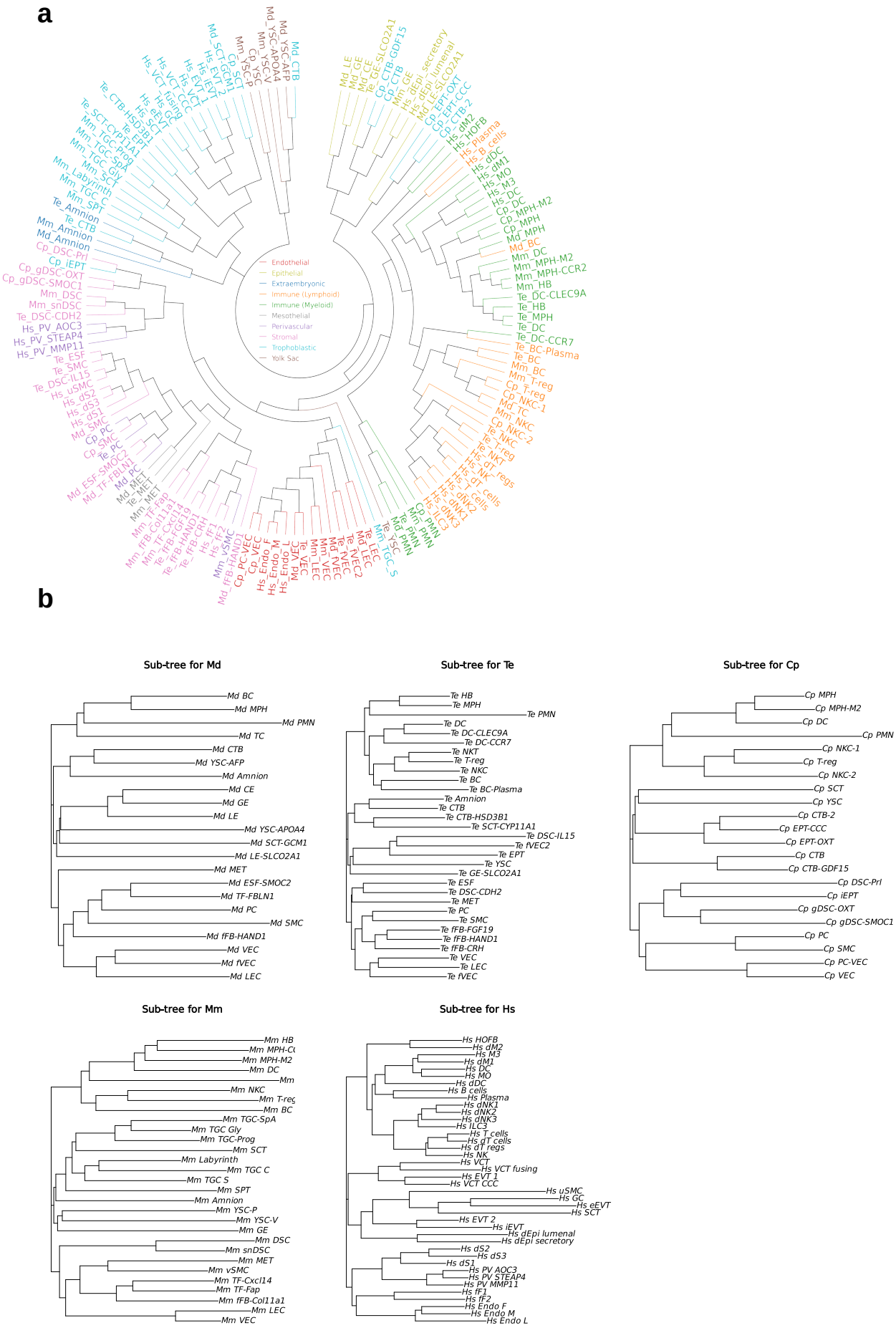

Figure S5. Cell type phylogenies of the cell types studied. **a.** Transcription factor-only cell phylogeny. **b.** Pruned trees from the all-genes tree (**Figure 1d**) showing within-species structure.

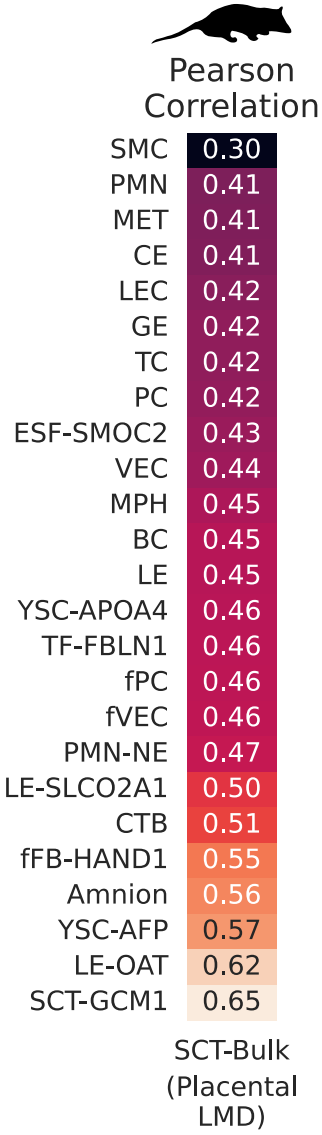

Figure S6. Laser microdissection verification of uncertain cell types, with Pearson correlations between micro-bulk transcriptomes and scRNA-seq clusters for opossum microdissected placenta from the bilaminar omphalopleure region (n=3)

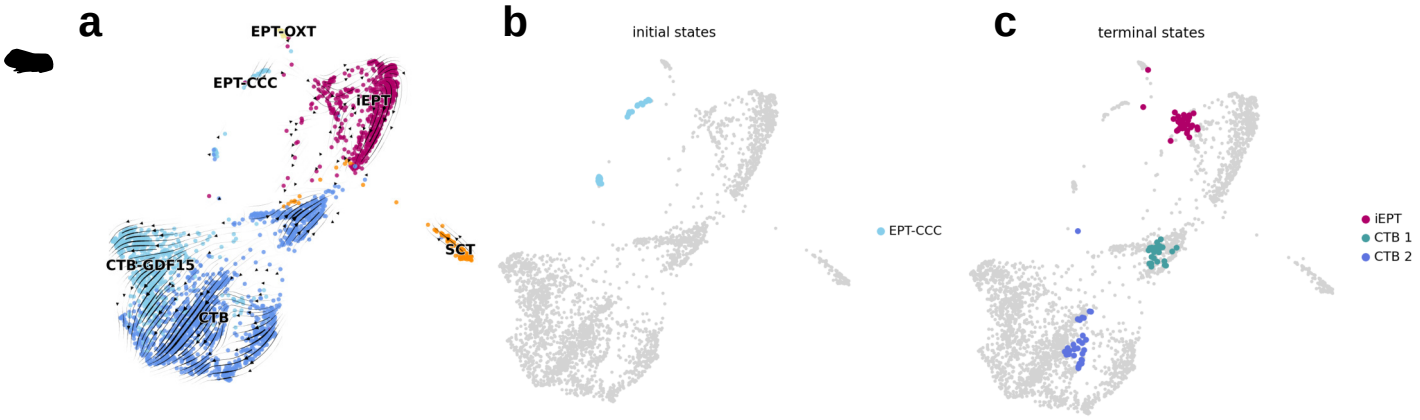

Figure S7. RNA velocity analysis of *Cavia* porcellus trophoblast. **a.** Force atlas embedding with velocity vectors for trophoblast cell types. **b-c.** Inferred initial **(b)** and terminal **(c)** states of placental cells based on RNA velocity-informed inference using CellRank.

a

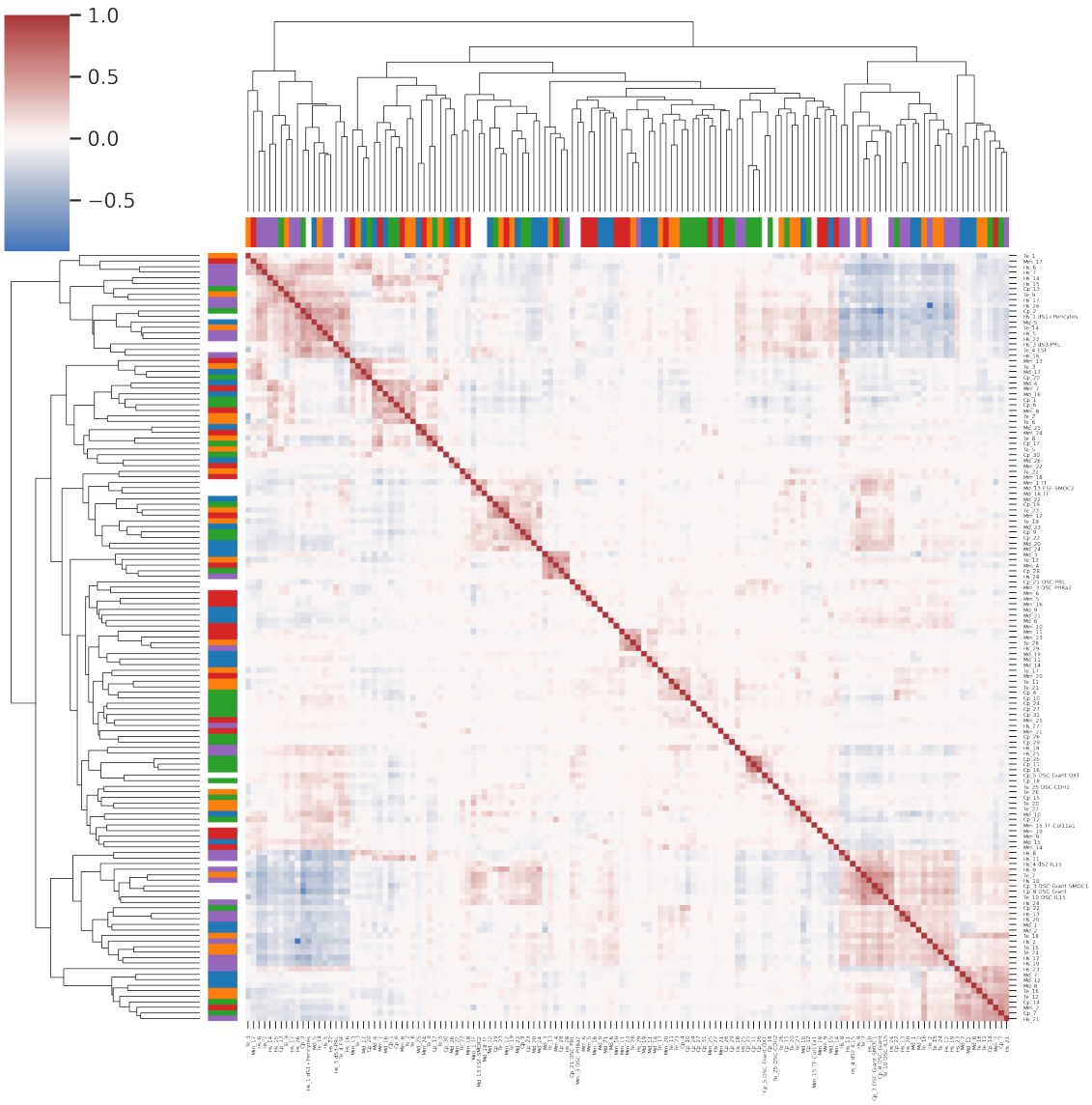

b

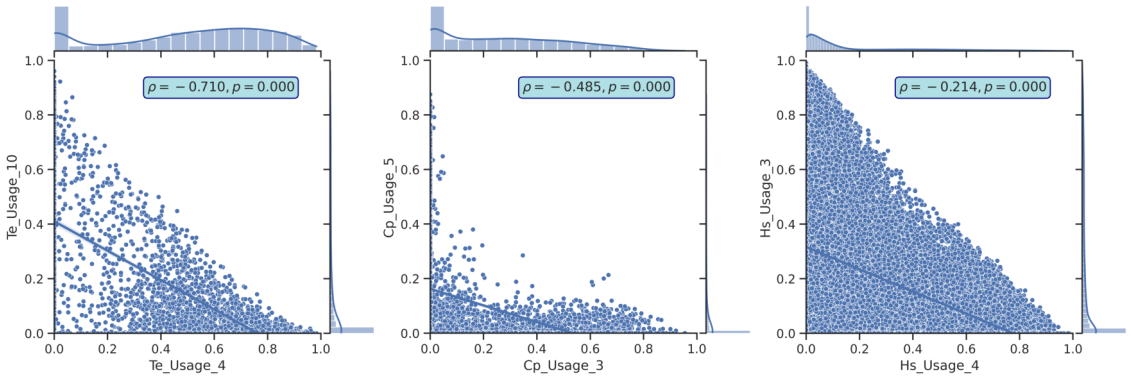

Figure S8. Cross-species NMF analysis. **a.** Correlation heatmap of cNMF gene expression programs from all species. **b.** “Type II” and “Type I” decidual gene expression program activity scores across individual stromal cells of tenrec (left), guinea pig (center), and human (right) show negative correlation, indicative of mutual exclusivity (i.e., cells expressing a “Type II” decidual program tend to not express “Type I”, and vice versa).

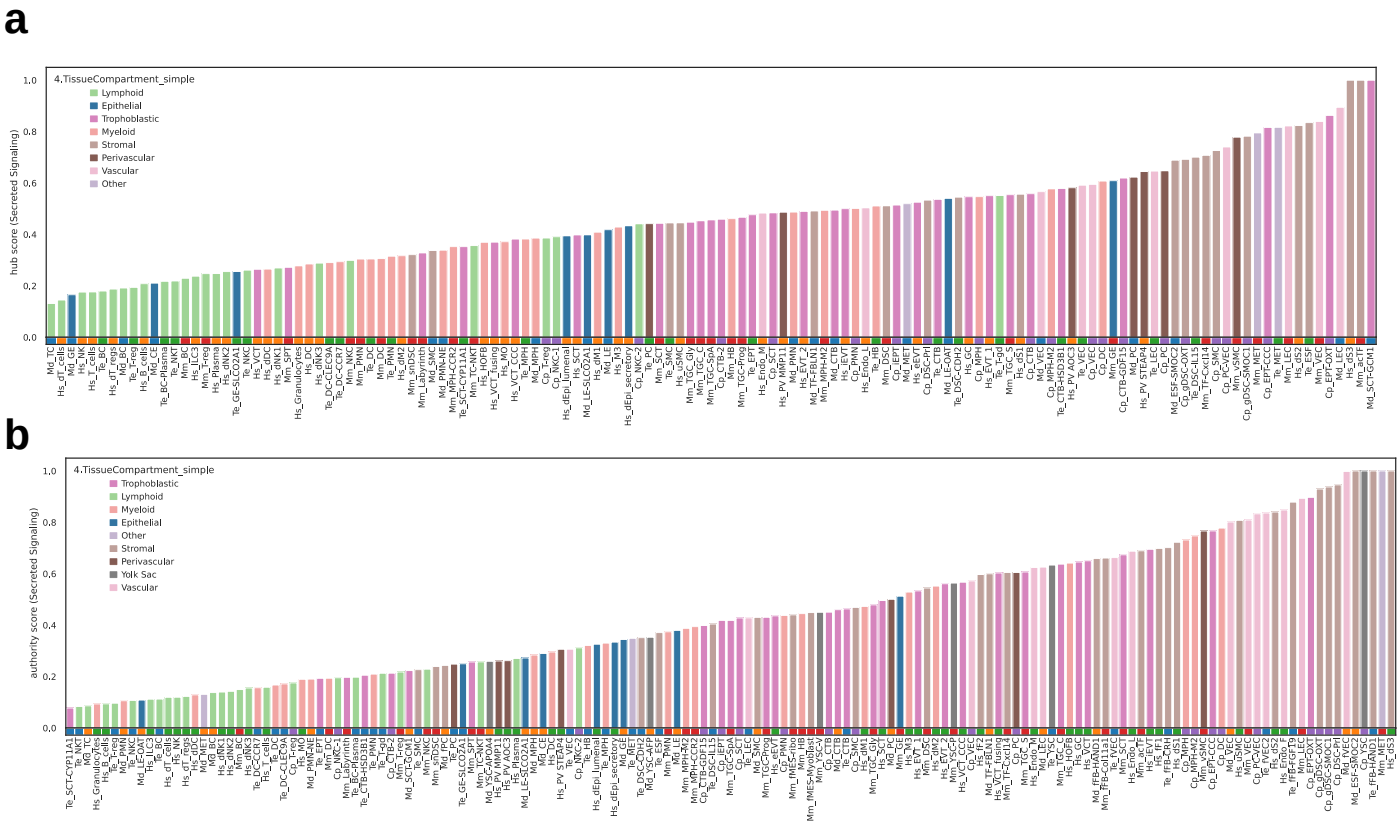

Figure S9. Graph statistics across cell types. Signaling graphs subset to interactions classified as secreted, peptide-mediated signals. Bars are colored by cell type family. **a.** HITS hub scores (a measure of outgoing signaling). **b.** HITS authority scores (a measure of incoming signaling potency). Scores are weighted by the LIANA+ “expr_prod” metric (a product of log-normalized expression values of ligand and receptor mRNA).

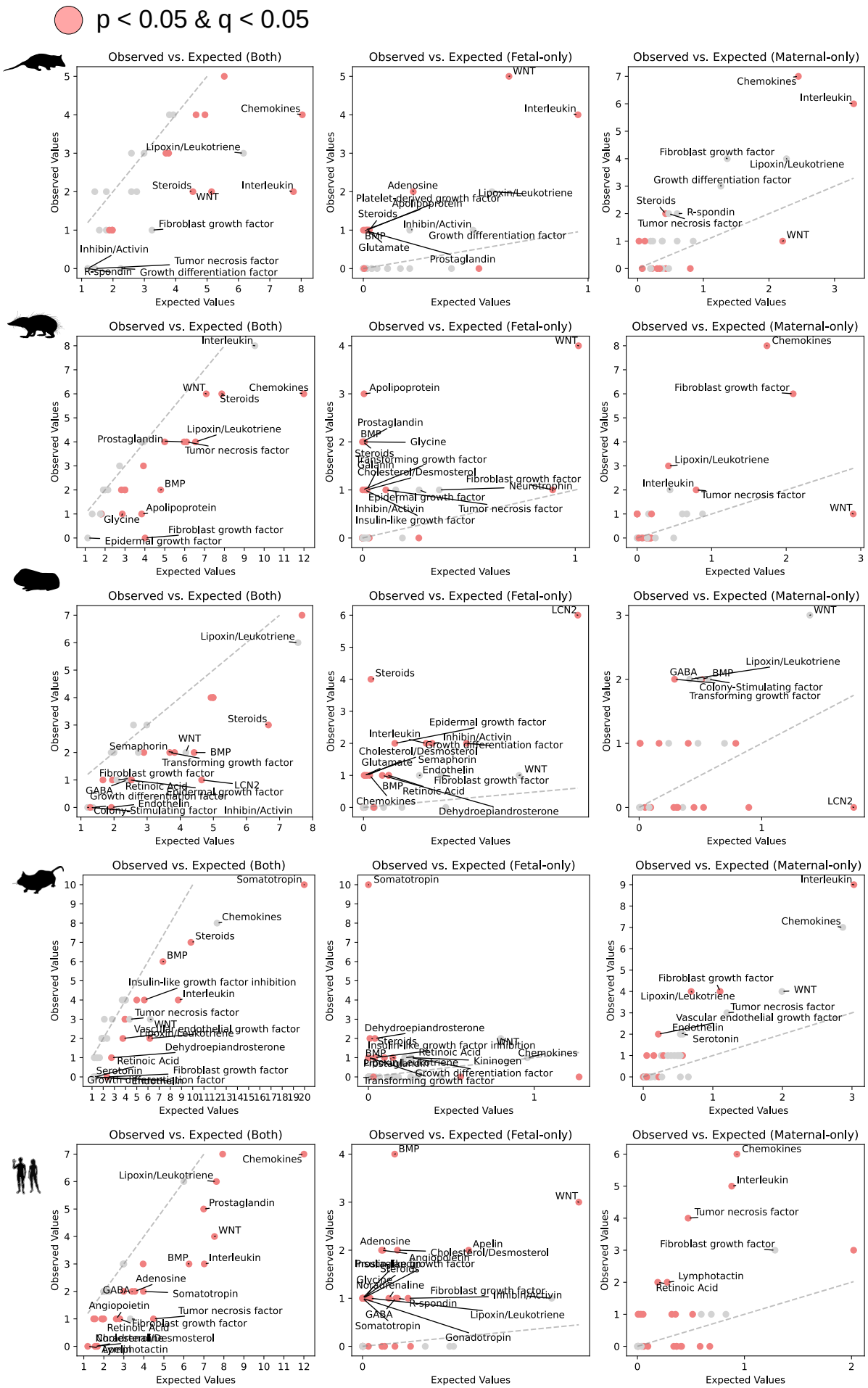

Figure S10. Disambiguation analysis. Observed versus expected numbers of interactions within a pathway which are ambiguous (left, expressed by both maternal and fetal cell types), fetal-only (middle), or maternal-only (right), for opossum, tenrec, guinea pig, mouse, and human. Pink shaded values indicate significance $p < 0.05$ and false discovery rate $q < 0.05$.

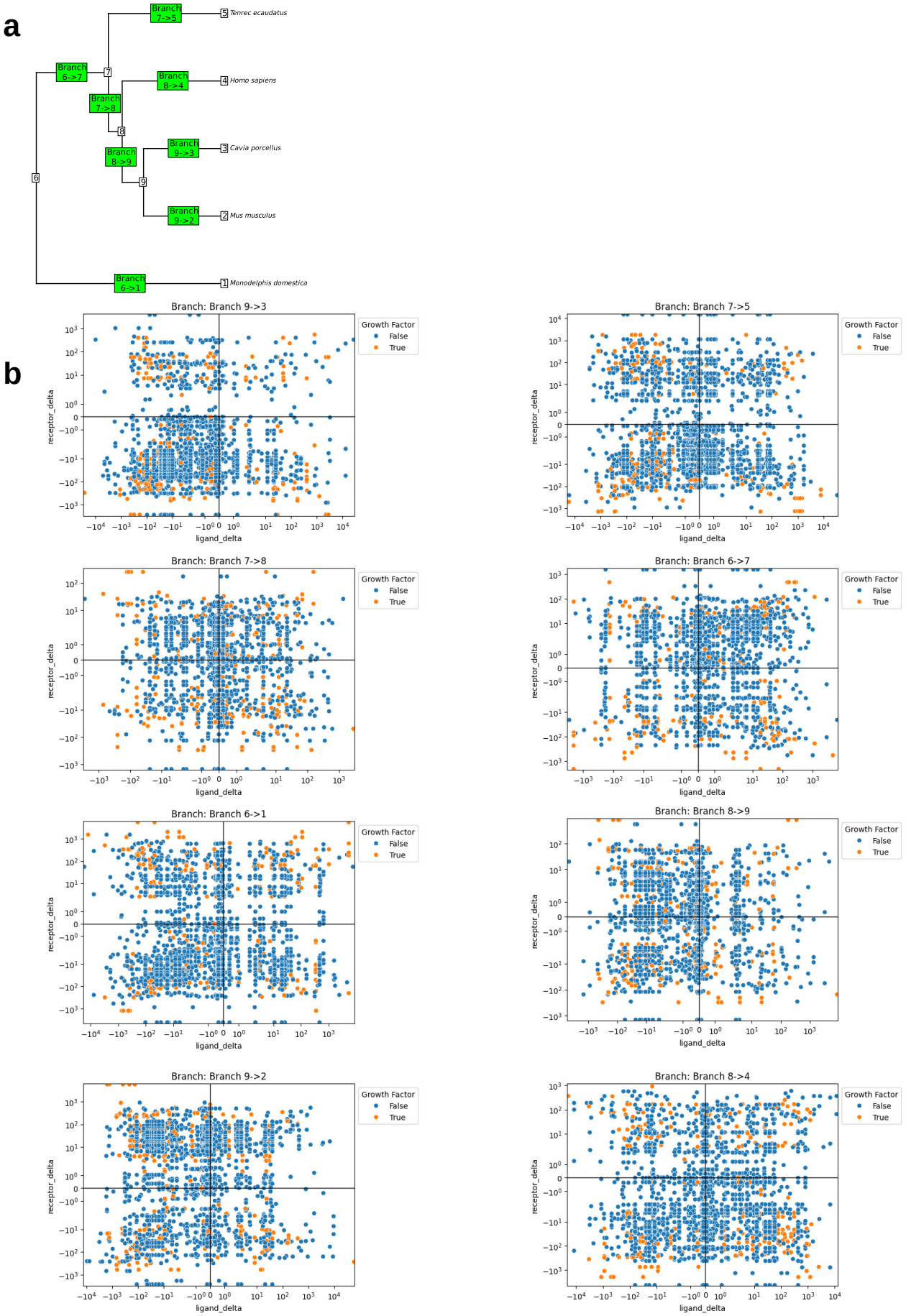

Figure S11. Test of the escalation hypothesis. **a.** Branch labels in the 5-species phylogeny of species sampled. **b.** Changes in inferred expression magnitude of placental ligands and cognate maternal receptors of secreted signals along internal branches of the 5-species phylogeny. Asymmetric changes fall into the upper-left and lower-right quadrants.

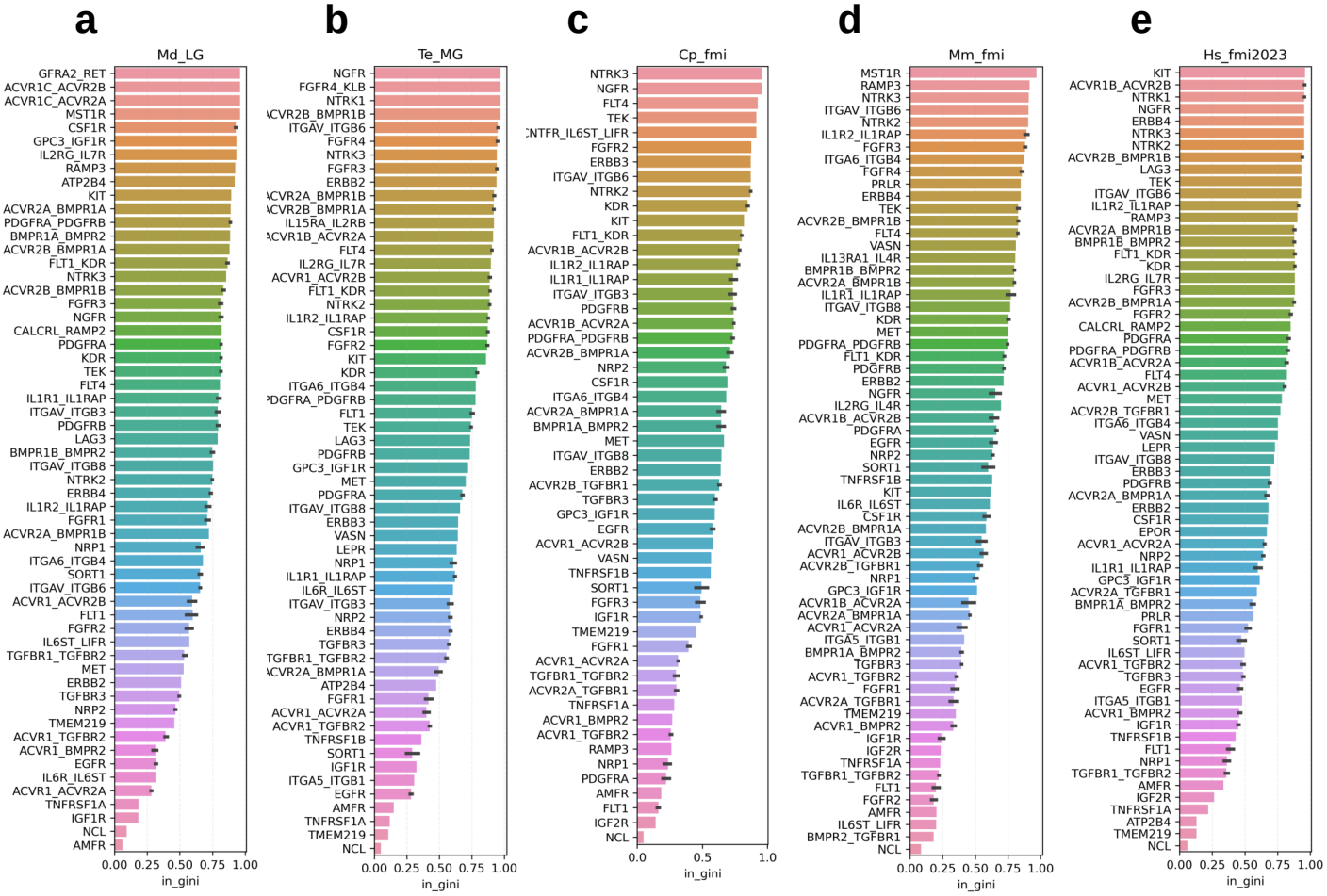

Figure S12. Quantification of cell type specificity of growth factor signaling ineractions in all species (**a:** *Monodelphis domestica*; **b:** *Tenrec ecaudatus*; **c:** *Cavia porcellus* **d:** *Mus musculus;* **e:** *Homo sapiens*). Gini indices of weighted in-degrees of signaling networks are reported, grouped by receptor. Error bars represent standard deviation of Gini indices for different ligands of that receptor, if the receptor utilizes multiple ligands in the augmented CellPhoneDB v5.0.0 ground truth interaction list (see Methods).

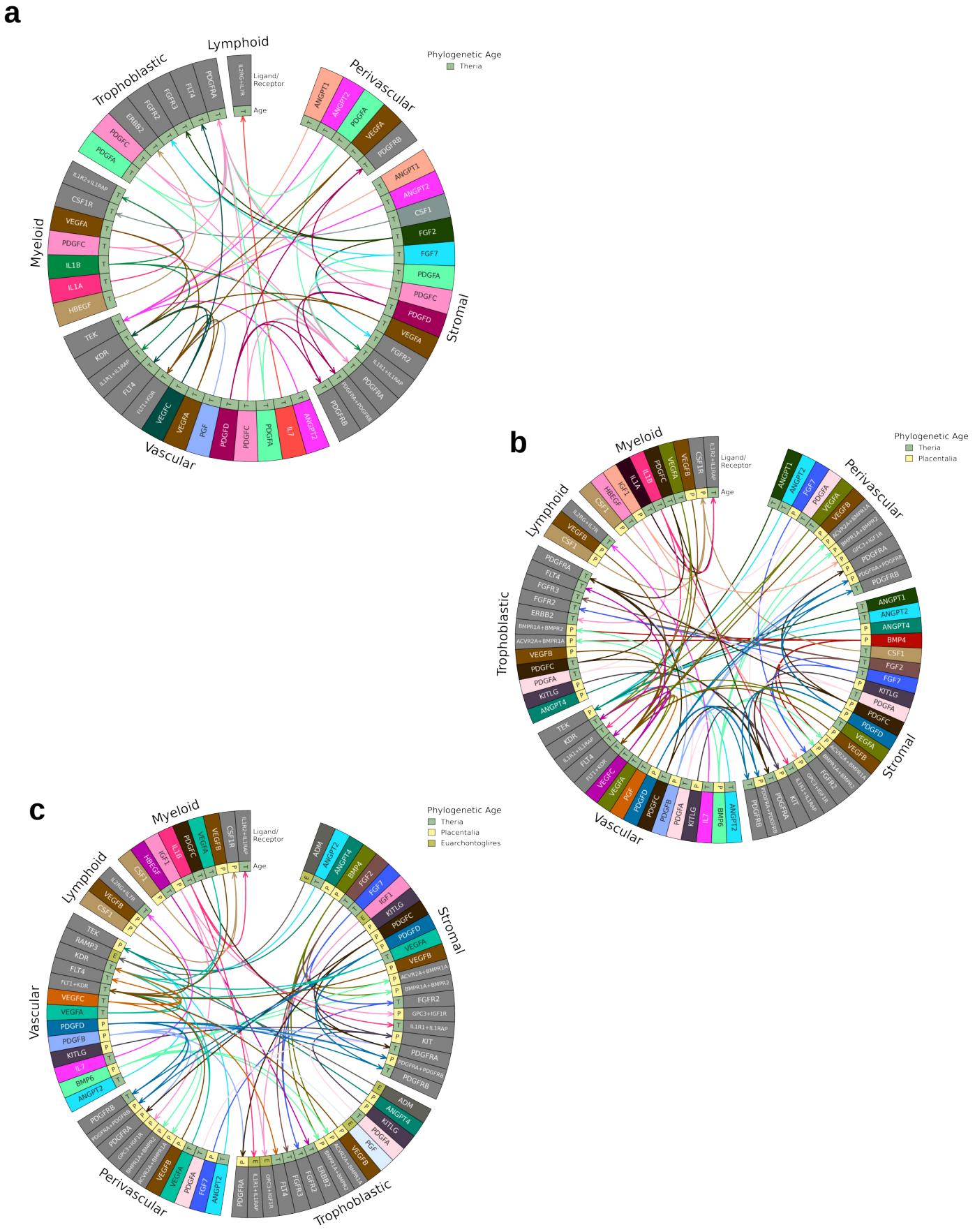

Figure S13. Lineage-specific growth factor signaling network between cell classes reconstructed in the most recent common ancestor of Theria (**a**) Placentalia (**b**) and Euarchontoglires (**c**). Interactions are annotated by phylogenetic age of first appearance.

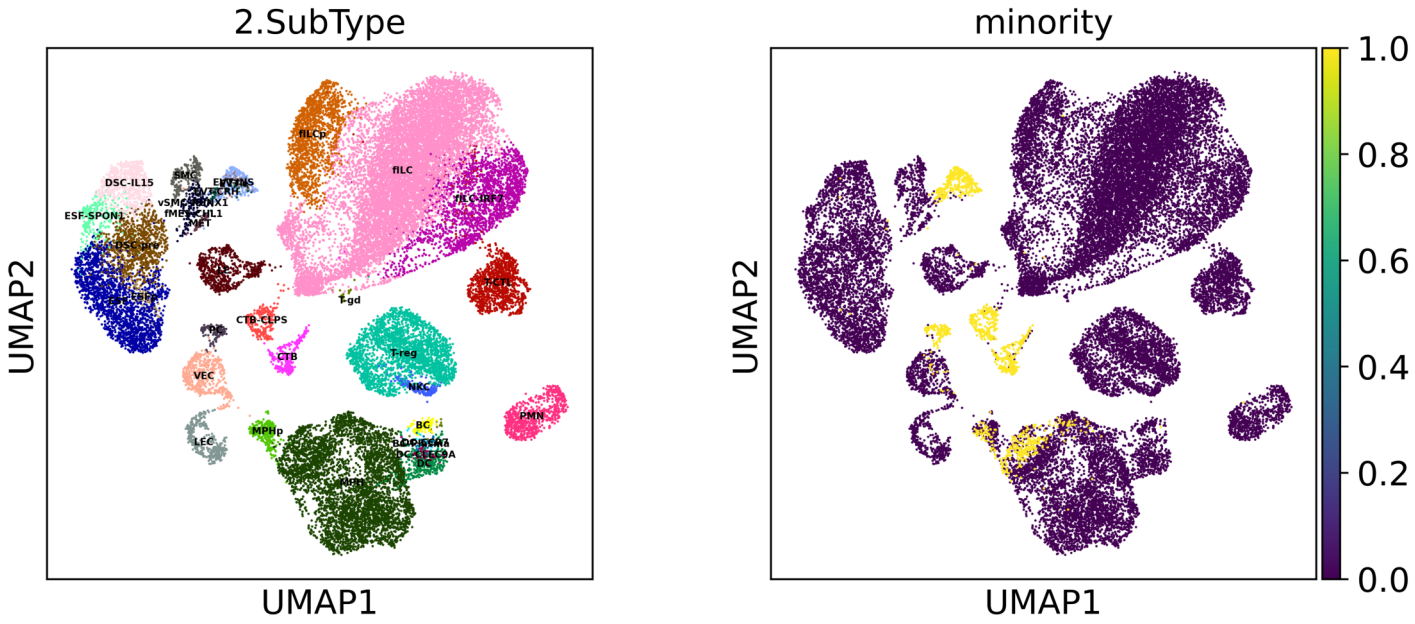

Figure S14. Souporcell calls for *Tenrec ecaudatus* (k=2 genomes). UMAP embeddings of all cells are shown, colored by cell subtype on the left, and by whether or not the cell was assigned to the less frequent genome (assumed fetal) by souporcell on the right. Souporcell minority clusters overap with those annotated as fetal by differential gene expression, and additionally facilitated the identification of hofbauer cells (fetal macrophages).